Mon. Not. R. Astron. Soc. **376,** 820–840 (2007) doi:10.1111/j.1365-2966.2007.11481.x

Interstellar medium oxygen abundances of dwarf irregular galaxies in Centaurus A and nearby groups⋆

Henry Lee,[1,2]† D. B. Zucker[3] and E. K. Grebel[4]

[1]*Gemini Observatory, Southern Operations Center, Casilla 603, La Serena, Chile*
[2]*Department of Astronomy, University of Minnesota, 116 Church St. S.E., Minneapolis, MN 55455, USA*
[3]*Institute of Astronomy, University of Cambridge, Madingley Road, Cambridge CB3 0HA*
[4]*Astronomical Institute, Department of Physics & Astronomy, University of Basel, Venusstrasse 7, CH-4102 Binningen, Switzerland*

Accepted 2007 January 8. Received 2007 January 7; in original form 2006 September 14

ABSTRACT

We present results of optical spectroscopy of 35 H II regions from eight dwarf galaxies in the Centaurus A (Cen A) group. [O III] λ4363 is detected in ESO272−G025 and ESO324−G024, and direct oxygen abundances of $12 + \log(\mathrm{O/H}) = 7.76 \pm 0.09$ and 7.94 ± 0.11 are derived, respectively. For the remaining galaxies, abundances are derived using common bright-line methods. To compare the influence of group environments on dwarf galaxies, we have also gathered data for additional dwarf irregular galaxies from the Cen A and the Sculptor groups from the literature. We have examined possible relationships between oxygen abundance, gas fraction, effective chemical yield and tidal indices. Despite large positive tidal indices for a number of Cen A dwarfs in the present sample, there is no clear separation between galaxies with positive tidal indices and galaxies with negative tidal indices in the luminosity–metallicity, metallicity–gas fraction and metallicity–tidal index diagrams. The H I surface mass density decreases with increasing positive tidal index, which is expected in strong tidal encounters. There are no strong trends between oxygen abundances or yields and projected distances of galaxies within their respective groups. We also present spectra for 13 H II regions in three nearby dwarf irregular galaxies: DDO 47, NGC 3109 and Sextans B. For DDO 47, the [O III] λ4363 oxygen abundance (7.92 ± 0.06) for the H II region SHK91 No. 18 agrees with recently published values. For Sextans B, the [O III] λ4363 oxygen abundance (7.80 ± 0.13) for H II region SHK91 No. 5 agrees with published work in which O^+ abundances were determined entirely from [O II] λλ7320, 7330 fluxes.

Key words: galaxies: abundances – galaxies: dwarf – galaxies: evolution – galaxies: interactions – galaxies: irregular.

1 INTRODUCTION

The problem of the formation and evolution of dwarf galaxies has partly been motivated by the long-standing questions about possible connections and transformations between different types of dwarf galaxies. The two basic morphological types are gas-poor dwarf spheroidals with very little present-day star formation, and gas-rich dwarf irregulars (dIs) and blue compact dwarf galaxies which contain recent bursts of star formation. Intrinsic properties (e.g. total mass) and external forces (e.g. environment) all have a role to play, but key processes may be difficult to identify and disentangle (e.g. Bothun et al. 1986; Grebel 1997, 1999; Grebel, Gallagher & Harbeck 2003; Lee, McCall & Richer 2003c; van Zee, Skillman & Haynes 2004a; van Zee, Barton & Skillman 2004b). The study of dwarf galaxies in different environments of varying galaxy number density (i.e. field, groups, clusters) provides valuable insights about the key parameters controlling evolution, and constraints to the various models for galaxy evolution.

1.1 Centaurus A group

The Centaurus A (Cen A) group is a loose collection of galaxies, and contains a very rich population of galaxies with the largest dispersion in morphological types (de Vaucouleurs 1979). The average distance of the Cen A group is comparable to that of the M81 group (cf. Karachentsev et al. 2002a; Karachentsev 2005). The Cen A group may already be virialized as indicated by the relatively short crossing time-scale (∼2–3 Gyr; Karachentsev 2005; Tully 2005).

⋆Based on EFOSC2 observations collected at the European Southern Observatory, Chile: proposal #70.B-0180(B).

†E-mail: hlee@gemini.edu

The Cen A group is separated into two 'subgroups' (Karachentsev et al. 2002b, their fig. 1) with one collection of galaxies surrounding NGC 5128 and the other collection surrounding the spiral galaxy M83. The M83 collection is more compact and contains more late-type galaxies, whereas the NGC 5128 collection is more dispersed and contains fewer late-type galaxies. The NGC 5128 subgroup has a heliocentric velocity $v_{\odot} = +312\,\mathrm{km\,s^{-1}}$ and an average distance $\langle D \rangle = 3.66$ Mpc. There are 31 known members, of which 10 (32 per cent) are classified as late-type dwarf galaxies (RC3 morphological type $T > 8$; de Vaucouleurs et al. 1991). The M83 subgroup has $v_{\odot} = +308\,\mathrm{km\,s^{-1}}$ and an average distance $\langle D \rangle = 4.56$ Mpc. There are 19 known members, of which 12 (63 per cent) are classified as late-type dwarf galaxies ($T > 8$).

The Cen A group is uniquely dominated by NGC 5128 (Cen A), which is a large massive radio-loud elliptical galaxy (e.g. Meier et al. 1989). The remaining massive members in the group all exhibit disturbed morphologies or abnormal properties, suggestive of a recent infall episode in which a population of gas-rich dwarf galaxies has been accreted into the group (e.g. Graham 1979; van Gorkom et al. 1990; Mirabel et al. 1999). This is precisely the scenario presented by Peng et al. (2002), who discovered a long, thin, blue arc in the northeast halo of NGC 5128. This feature is thought to have once been a low-mass dI which fell into the halo of the elliptical and is undergoing tidal disruption. This may also help explain why there are relatively few dIs in the vicinity of NGC 5128, compared to M83 (Karachentsev et al. 2004).

Additional studies of dwarf galaxies in the Cen A group have been carried out in Hα (S. Côté et al., in preparation) and in H I (Côté et al. 1997; Banks et al. 1999; Côté, Carignan & Freeman 2000) to examine the total and spatial distribution of gas and recent star formation. Rejkuba et al. (2006) studied the red giant stellar populations in two Cen A dwarf elliptical galaxies, and found the fraction of intermediate-age stars to all stars is smaller than that found in Local Group dwarf ellipticals. Jerjen, Binggeli & Freeman (2000) identified 13 new dwarf elliptical galaxies, and confirmed the membership of two dwarf irregular galaxies in the group. They also identified AM 1318−444 and ESO 381−G018 as two new dwarf irregulars in the Cen A group. Grossi et al. (2007) examined three gas-rich dwarf spheroidals with old ($\gtrsim 2$ Gyr) stellar populations, and showed that the relatively high gas content could be explained by the low level of past star formation.

Oxygen abundances are a reliable measure of the present-day gas-phase metallicity within H II regions in gas-rich star-forming dwarf galaxies (e.g. Dinerstein 1990; Skillman 1998). In fact, they provide useful constraints as the most recent and maximum metallicity to anchor the star formation history. Webster & Smith (1983) and Webster et al. (1983) obtained oxygen abundances for southern irregular and spiral galaxies, including galaxies in the Cen A group and in the field, with a measured range of abundances from about 10 to 60 per cent of the solar value. Although these papers have been, until recently, the primary work regarding abundances in Cen A late-type dwarf galaxies, the spectra were obtained with inherently non-linear detectors. In many cases, the character of the non-linearities was not understood until after publication (e.g. Jenkins 1987); subsequent corrections for non-linearity were not possible.

For a comparison of gas-phase abundances with published work on nearby dwarf galaxies (e.g. Skillman, Côté & Miller 2003b; Lee & Skillman 2004; Lee, Skillman & Venn 2005, 2006a; van Zee, Skillman & Haynes 2006), we undertook a program of determining new and confirming previous nebular oxygen abundances for gas-rich dwarf galaxies in the Local Volume (Grebel et al. 2000), which would help answer the question about whether recent chemical enrichment is sensitive to the (group) environment. Here, we present spectra of 35 H II regions in eight Cen A dIs, as well as spectra of 13 H II regions in three additional nearby dwarf galaxies. The properties of galaxies in the present sample are listed in Table 1.

The paper is organized as follows. Observations and reductions of the data are presented in Section 2, the measurements and analyses are given in Section 3, derivations of chemical abundances are described in Section 4, individual galaxies are presented in Section 5, a discussion of environmental effects is given in Section 6 and the conclusions are given in Section 7. For the remainder of this paper, we adopt $12 + \log(\mathrm{O/H}) = 8.66$ as the revised solar value for the oxygen abundance, and $\mathrm{Z}_{\odot} = 0.0126$ as the revised solar mass fraction in the form of metals (Asplund et al. 2004; Meléndez 2004).

2 OBSERVATIONS AND REDUCTIONS

Long-slit spectroscopic observations were carried out on 2003 March 6-8 UT with the EFOSC2 imaging spectrograph on the 3.6-m telescope at ESO La Silla Observatory. Details of the instrumentation employed and the log of observations are listed in Tables 2 and 3, respectively. Observations were obtained just after new moon phase. Conditions were mostly clear on the first two nights with patchy thin cloud towards the end of the second night; the third night was clear and photometric.

3- to 5-min Hα acquisition images were obtained in order to position the slit. The slit angle was aligned to obtain spectra of multiple H II regions. H II region targets for each galaxy are shown in Figs 1 and 2. Identifications and locations of various H II regions in each target are labelled. The acquisition images were obtained in 'fast' readout mode, which is about a factor of 2 faster in readout time than 'normal' mode. However, two different amplifiers are used during 'fast' readout, which causes different characteristics for the two halves of the CCD detector. The 'split' appearance was corrected by adding a constructed image with zeros on one-half of the frame and the average zero-point difference on the other half of the frame. All subsequent science exposures (biases, flats, arcs, targets) were obtained in 'normal' readout.

Data reductions were carried out using standard IRAF[1] routines. Data obtained on each separate night were reduced independently. The raw two-dimensional images were bias subtracted and trimmed. Dome flat exposures were used to remove pixel-to-pixel variations in response, and twilight flats were acquired at dusk each night to correct for variations over larger spatial scales. To correct for the 'slit function' in the spatial direction, the variation of illumination along the slit was taken into account using dome and twilight flats. Cosmic rays were removed in the addition of multiple exposures. Wavelength calibration was obtained using helium–argon (He–Ar) arc lamp exposures taken throughout each night. Flux calibration was obtained using exposures of standard stars CD−32° 9927, Feige 56, LTT 1788 and LTT 3864. The flux accuracy is listed in Table 3. One-dimensional spectra for each H II region were obtained with unweighted summed extractions. Some of the spectra are shown in Fig. 3.

The [O II] λλ7320, 7330 doublet was detected and reported in a number of spectra below. However, we did not use an ultraviolet-cut-off filter, and we caution the reader that the reported [O II] λλ7320,

[1] IRAF is distributed by the National Optical Astronomical Observatories, which is operated by the Associated Universities for Research in Astronomy, Inc., under contract to the National Science Foundation.

Table 1. Basic properties of galaxies in the present sample. Galaxies are listed in alphabetical order by their primary name. All properties are obtained from NED, unless otherwise noted. Columns (1) and (2): galaxy name used in the present work, and other names from NED, respectively. Column (3): morphological type (de Vaucouleurs et al. 1991). Column (4): heliocentric velocity. Column (5): total apparent B magnitude. Column (6): total H I 21-cm flux; additional reference: Karachentsev et al. (2004). Column (7): measured or estimated distances. References: Centaurus A group galaxies – Karachentsev et al. (2002b, 2004, 2006); DDO 47 – Karachentsev et al. (2003b); NGC 3109 – Karachentsev et al. (2002c); Sextans B – Sakai, Madore & Freedman (1997), Karachentsev et al. (2002c). Column (8): method of determining distances: TRGB – tip of the red giant branch; HF – Hubble flow. Columns (9) and (10): tidal index and 'closest' or main disturber (MD) galaxy, respectively (Karachentsev et al. 2004). Column (11): nebular oxygen abundances derived in the present work.

Galaxy (1)	Other name(s) (2)	T (3)	$v_\odot$ (km s^{-1}) (4)	B_T (mag) (5)	F_{21} (Jy km s^{-1}) (6)	D (Mpc) (7)	Method (8)	Θ (9)	MD (10)	12+ log(O/H) (11)
Centaurus A group dwarfs										
AM 1318−444	KK 196	10	+741	16.1	...	3.98 ± 0.32	TRGB	+2.2	Cen A	7.87 ± 0.20
AM 1321−304	KK 200, KDG 15	9	+490	16.67	1.7	4.63 ± 0.46	TRGB	+1.2	M 83	...
ESO 272−G025	PGC 52591	8	+624	14.79	3.0	5.9	HF	−1.5	Cen A	7.76 ± 0.09
ESO 274−G001	UKS 1510−466	7	+522	11.70	117[a]	3.05 ± 0.24	TRGB	−1.0	Cen A	8.38 ± 0.20
ESO 321−G014	AM 1211−375	10	+613	15.16	2.9	3.19 ± 0.26	TRGB	−0.3	Cen A	...
ESO 324−G024	AM 1324−411	10	+513	12.91	52.1[a]	3.73 ± 0.43	TRGB	+2.4	Cen A	7.94 ± 0.18
ESO 325−G011	AM 1342−413	10	+541	13.99	25.4[a]	3.40 ± 0.39	TRGB	+1.1	Cen A	7.94 ± 0.20
ESO 381−G020	AM 1243−333	10	+590	14.44	36[b]	5.45 ± 0.44	TRGB	−0.3	M 83	7.90 ± 0.20
IC 4247	ESO 444−G034	10	+274	14.41	3.0	4.97 ± 0.40	TRGB	+1.5	M 83	8.27 ± 0.20
IC 4316	ESO 445−G006	10	+674	14.97	7.8[a]	4.41 ± 0.44	TRGB	+2.4	M 83	8.16 ± 0.20
Nearby dwarfs										
DDO 47	UGC 3974	10	+ 272	13.60	67.0[c]	5.18 ± 0.57	TRGB	−2.1	NGC 2683	7.92 ± 0.06
NGC 3109[d]	DDO 236	9	+404	10.26	1110[e]	1.33 ± 0.08	TRGB	−0.1	Antlia	7.94 ± 0.20
Sextans B[d]	DDO 70, UGC 5373	10	+301	11.85	102.4[c]	1.36 ± 0.07	TRGB	−0.7	MWay	7.80 ± 0.13

Notes: [a]From Côté et al. (1997). [b]From Banks et al. (1999). [c]From Hoffman et al. (1996). [d]Common group of dwarfs including NGC 3109, Sextans A, Sextans B and the Antlia dwarf (van den Bergh 1999; Tully et al. 2002). [e]From Barnes & de Blok (2001).

Table 2. Properties of EFOSC2 spectrograph employed at the ESO La Silla 3.6-m telescope.

CCD	Loral, No. 40
Total area	2048 × 2048 pix^2
Field of view	5.2 × 5.2 arcmin^2
Pixel size	15 μm
Image scale	0.157 arcsec pix^{-1}
Gain	1.3 e^- ADU^{-1}
Read-noise (rms)	8.5 e^-
Grating	No. 11
Groove density	300 lines mm^{-1}
Blaze λ (1st order)	4000 Å
Dispersion	2.0 Å pix^{-1}
Effective λ range	3380–7520 Å
Long-slit length	≃5 arcmin
Slit width	1 arcsec

7330 fluxes may suffer from second-order contamination. In the present work, we used only [O II] λ3727 to derive O^+/H ionic abundances and total oxygen abundances.

3 MEASUREMENTS AND ANALYSIS

Emission-line strengths were measured using software developed by M. L. McCall and L. Mundy; see (Lee, Grebel & Hodg 2003a,b,c). The temperature-sensitive [O III] λ4363 emission line was detected in four galaxies: DDO 47 (H II region SHK91 No. 18), ESO 272−G025 (H II region No. 1), ESO 324−G024 (H II region No. 4) and Sextans B (H II region SHK91 No. 5).

We have followed the general procedure described in Lee & Skillman (2004) and Lee et al. (2005, 2006a). To derive reddening values, Hα and Hβ fluxes were used with the following

$$\log \frac{I(\lambda)}{I(\mathrm{H}\beta)} = \log \frac{F(\lambda)}{F(\mathrm{H}\beta)} + c(\mathrm{H}\beta)\, f(\lambda), \quad (1)$$

where F and I are the observed flux and corrected intensity ratios, respectively, $c(\mathrm{H}\beta)$ is the logarithmic extinction at Hβ and $f(\lambda)$ is the wavelength-dependent reddening function (Aller 1984; Osterbrock 1989). The logarithmic extinction can be expressed as

$$c(\mathrm{H}\beta) = 1.43\, E(B-V) = 0.47\, A_V, \quad (2)$$

where $E(B-V)$ is the reddening and A_V is the extinction in V. Intrinsic case-B Balmer line ratios determined by Storey & Hummer (1995) were assumed. In the absence of Hδ, a best solution to the expected $I(\mathrm{H}\alpha)/I(\mathrm{H}\beta)$ and $I(\mathrm{H}\gamma)/I(\mathrm{H}\beta)$ intensity ratios was obtained simultaneously. Only the $F(\mathrm{H}\alpha)/F(\mathrm{H}\beta)$ flux ratio was used to determine a reddening in the absence of both Hγ and Hδ. An initial temperature $T_e = 10^4$ K was used to derive the reddening. As the [S II] λλ6716, 6731 lines were generally unresolved, $n_e = 100\,\mathrm{cm}^{-3}$ was adopted for the electron density.

The reddening function normalized to Hβ is derived from the Cardelli, Clayton & Mathis (1989) reddening law, assuming $R_V = 3.07$. As described in Skillman et al. (2003b), values of $c(\mathrm{H}\beta)$ were derived from the error weighted average of values for $F(\mathrm{H}\alpha)/F(\mathrm{H}\beta)$, $F(\mathrm{H}\gamma)/F(\mathrm{H}\beta)$ and $F(\mathrm{H}\delta)/F(\mathrm{H}\beta)$ ratios while simultaneously solving for the effects of underlying Balmer absorption with equivalent width, $\mathrm{EW_{abs}}$. We assumed that $\mathrm{EW_{abs}}$

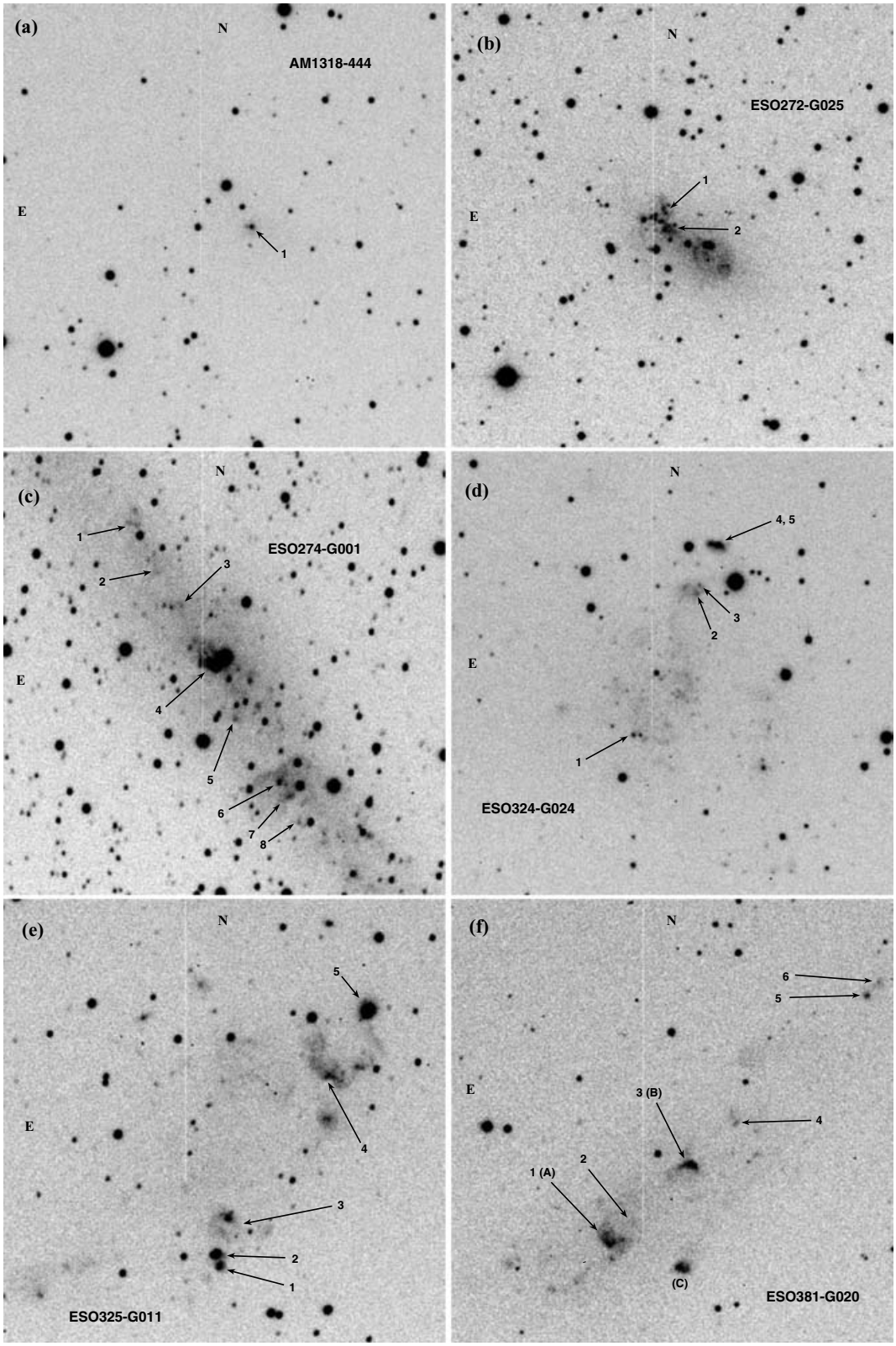

Figure 1. Raw (unreduced) Hα acquisition images in 3-min exposures taken with EFOSC2. Black objects indicate bright sources. North and east are to the top and the left, respectively, in each frame. Thin white stripes in the frames indicate bad rows or columns. Numbers in each panel indicate the locations of extracted H II region spectra tabulated in Tables 4 to 11. All images shown have approximately 1.6×1.3 arcmin^2 fields of view. (a) AM1318−444. (b) ESO 272−G025. (c) ESO 274−G001. (d) ESO 324−G024. (e) ESO 325−G011. (f) ESO 381−G020. H II regions 1 and 3 correspond to H II regions A and B, respectively, from Webster et al. (1983); their H II region C is the dark blob to the southwest of H II region 1.

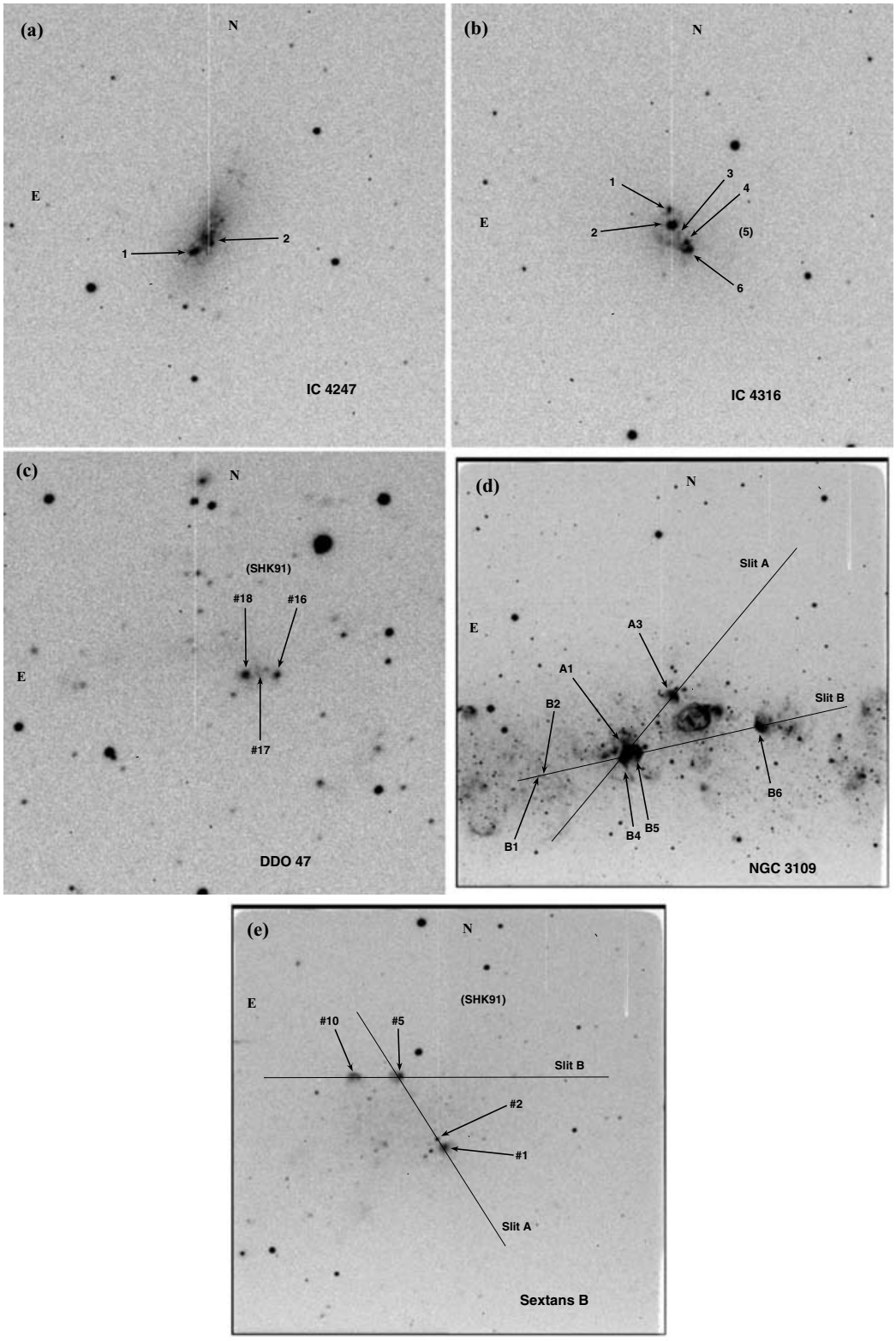

Figure 2. Additional Hα acquisition images. (a) IC 4247. (b) IC 4316. (c) DDO 47. (d) NGC 3109 (approx. 5.2 × 5.2 arcmin^2 field of view). (e) Sextans B (approx. 5.2 × 5.2 arcmin^2 field of view). See Fig. 1 for additional comments.

was the same for Hα, Hβ, Hγ and Hδ. Uncertainties in c(Hβ) and EW$_{\rm abs}$ were determined from Monte Carlo simulations (Olive & Skillman 2001; Skillman et al. 2003b). Errors derived from these simulations are larger than errors quoted in the literature by either assuming a constant value for the underlying absorption or derived from a χ^2 analysis in the absence of Monte Carlo simulations for the errors; Fig. 4 shows an example of these simulations.

Table 3. Log of observations. Column (1): galaxy name (in alphabetical order). Column (2): date of observation. Column (3): number of exposures obtained and the length of each exposure in seconds. Column (4): total exposure time. Column (5): mean effective air mass. Column (6): [O III] λ4363 detection. Column (7): relative root-mean-square error in the sensitivity function obtained from observations of standard stars.

Galaxy (1)	2003 Date (UT) (2)	N_{exp} (3)	t_{total} (s) (4)	$\langle X \rangle$ (5)	[O III] λ4363 (6)	RMS (mag) (7)
AM 1318−444	7 March	3 × 1200 + 1 × 1800	5400	1.11	...	0.021
AM 1321 − 304[a]	7 March	...	...	...	...	...
DDO 47	7 March	4 × 1200	4800	1.44	Yes	0.021
ESO 272−G025	6 March	5 × 1200	6000	1.04	Yes	0.021
ESO 274−G001	8 March	4 × 600	2400	1.05	...	0.024
ESO 321−G014[b]	6 March	1 × 1200	1200	...	...	...
ESO 324−G024	7 March	4 × 1200	4800	1.02	Yes	0.021
ESO 325−G011	8 March	3 × 1200	3600	1.04	...	0.024
ESO 381−G020	8 March	2 × 1200	2400	1.22	...	0.024
IC 4247	8 March	3 × 1200	3600	1.17	...	0.024
IC 4316	6 March	4 × 1200	4800	1.03	...	0.021
NGC 3109 slit A	7 March	4 × 1200	4800	1.01	...	0.021
NGC 3109 slit B	8 March	4 × 1200	4800	1.10	...	0.024
Sextans B slit A	6 March	3 × 1200	3600	1.43	...	0.021
Sextans B slit B	6 March	1 × 548 + 4 × 1200	5348	1.23	Yes	0.021

Notes: [a]No compact Hα emission observed in a 3-min acquisition frame. [b]Faint diffuse Hα emission. The long-slit was placed along major axis of the galaxy, but no emission lines were seen.

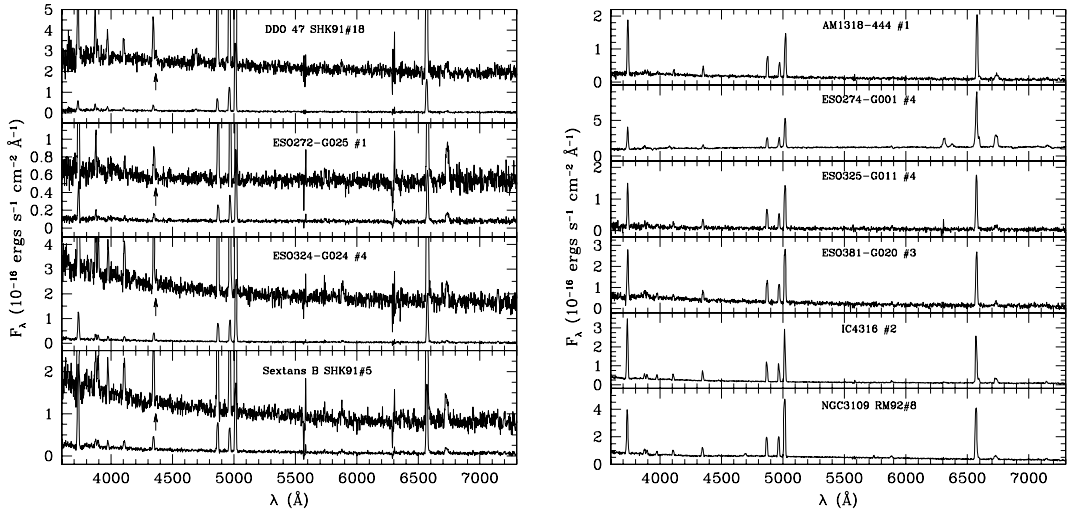

Figure 3. Left-hand panel: [O III] λ4363 detections: DDO 47 SHK91 No. 18, ESO 272−G025 No. 1, ESO 324−G024 No. 4 and Sextans B SHK91 No. 5. The SHK identifications for H II regions are found in Strobel, Hodge & Kennicutt (1991). The observed flux per unit wavelength is plotted versus wavelength. Within each panel, the full spectrum and an expanded view of the spectrum to highlight faint emission lines are shown. The [O III] λ4363 line is indicated by an arrow in each panel. Right-hand panel: other example H II region spectra for AM 1318−444 No. 1, ESO 274−G001 No. 4, ESO 325−G01 No. 4, ESO 381−G020 No. 3, IC 4316 No. 2 and NGC 3109 RM92 No. 8. RM92 refers to Richer & McCall (1992).

Observed flux (F) and corrected intensity (I) ratios, observed Hβ fluxes, logarithmic reddening values and the equivalent widths of underlying Balmer absorption are listed in Tables 4 to 12 inclusive. The listed errors for the observed flux ratios at each wavelength λ account for the errors in the fits to the line profiles, their surrounding continua and the relative error in the sensitivity function stated in Table 3. At the Hβ reference line, errors for both observed and corrected ratios do not include the error in the flux. Where negative values of the reddening were derived, the reddening was set to zero in correcting line ratios and in abundance calculations. Where [O III] λ4363 is absent, we have assumed a fiducial temperature of $T_e = 10^4$ K, and, in a number of cases, we have also assumed 2 Å for the equivalent width of the underlying Balmer absorption.

He II λ4686 emission was detected in H II regions DDO 47 SHK91 No. 18 and NGC 3109 RM92 No. 8 (A1). The equivalent widths of the He II λ4686 emission line are 9.2 ± 1.7 and 5.05 ± 0.45 Å, respectively. The corresponding fluxes are between 1 and 3 × 10^{-16} erg s^{-1} cm^{-2} (Fig. 5; Tables 10 and 11), and I(He II)/I(Hβ) values are about 10 per cent. These values are unusually high compared to predictions from models of young stellar populations in recent starbursts (e.g. Schaerer & Vacca 1998). In particular,

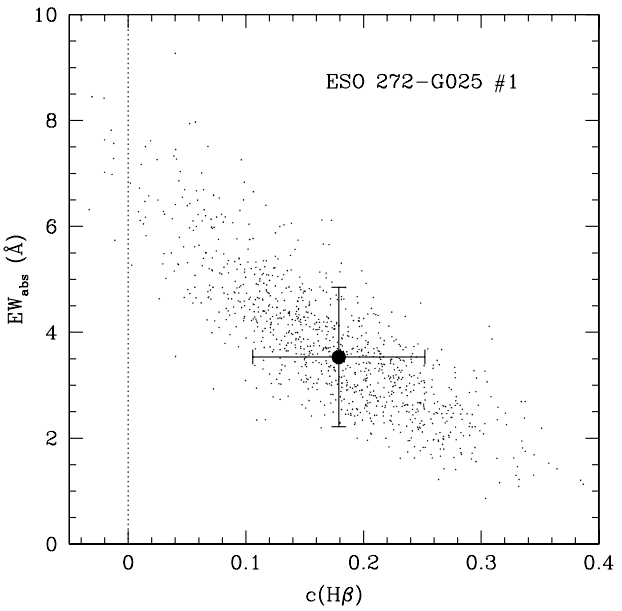

Figure 4. Monte Carlo simulations of solutions for the reddening, $c(\mathrm{H}\beta)$, and the underlying Balmer absorption with equivalent width, $\mathrm{EW_{abs}}$, from hydrogen Balmer flux ratios. The dotted line indicates zero reddening. The results here are shown for the H II region ESO 272−G025 No. 1. Each small point is a solution derived from a different realization of the same input spectrum. The large filled circle with error bars shows the mean result with 1σ errors derived from the dispersion in the solutions.

the $I(\mathrm{He\,II})/I(\mathrm{H}\beta)$ values do not agree with a relatively metal-poor ($Z = 0.004$) burst with a Salpeter stellar initial mass function (upper limit $120\,\mathrm{M}_\odot$), and an instantaneous burst of star formation with ages $\lesssim$10 Myr. Shocks from supernovae are an unlikely contributor to the He II emission, as [O I] emission (e.g. Skillman 1985) is not present in the spectra.

4 NEBULAR ABUNDANCES

Oxygen abundances in H II regions were derived using three methods: (1) the direct method (e.g. Dinerstein 1990; Skillman 1998); and two bright-line methods discussed by (2) McGaugh (1991), which is based on photoionization models and (3) Pilyugin (2000), which is purely empirical. We briefly summarize these methods here; further details of these methods are found in Lee & Skillman (2004) and Lee et al. (2005, 2006a).

4.1 Direct ([O III] λ4363) abundances

The 'direct' conversion of emission-line intensities into ionic abundances requires a reliable estimate of the electron temperature in the ionized gas. We adopt a two-zone model for H II regions, with a low- and a high-ionization zone characterized by temperatures $T_\mathrm{e}(\mathrm{O}^+)$ and $T_\mathrm{e}(\mathrm{O}^{+2})$, respectively. The temperature in the O^{+2} zone is measured with the emission line ratio I([O III] λ5007)/I([O III] λ4363) (Osterbrock 1989). The temperature in the O^+ zone is given by

$$t_\mathrm{e}(\mathrm{O}^+) = 0.7\,t_\mathrm{e}(\mathrm{O}^{+2}) + 0.3, \quad (3)$$

where $t_\mathrm{e} = T_\mathrm{e}/10^4$ K (Campbell, Terlevich & Melnick 1986; Garnett 1992).

The total oxygen abundance by number is given by $\mathrm{O/H} = \mathrm{O}^+/\mathrm{H}^+ + \mathrm{O}^{+2}/\mathrm{H}^+$. For conditions found in typical H II regions and those presented here, very little oxygen in the form of neutral oxygen is expected, and is not included here. Ionic abundances for singly- and doubly ionized oxygen were computed using O^+ and O^{+2} temperatures, respectively, as described above. The O^{+3} contribution is assumed negligible where He II emission is absent. Although He II emission is reported in two H II regions (see above), we have not included the small contribution by O^{+3} to the total oxygen abundance.

In four of the 48 H II region spectra, [O III] λ4363 line fluxes were measured, and subsequent electron temperatures were derived. We derived direct oxygen abundances in H II regions with [O III] λ4363 detections using the method described by Skillman et al. (2003b). Ionic and total abundances are computed using the emissivities from the five-level atom program by Shaw & Dufour (1995). As described above, we use the same two-temperature zone model and temperatures for the remaining ions. The error in $T_\mathrm{e}(\mathrm{O}^{+2})$ is derived from the uncertainties in the corrected emission-line ratios, and does not include any uncertainties in the atomic data, or the possibility of temperature variations within the O^{+2} zone. The fractional error in $T_\mathrm{e}(\mathrm{O}^{+2})$ is applied similarly to $T_\mathrm{e}(\mathrm{O}^+)$ to compute the uncertainty in the latter. Uncertainties in the resulting ionic abundances are combined in quadrature for the final uncertainty in the total linear (summed) abundance. The appropriate temperatures, [O III] λ4363 abundances, and their uncertainties are listed in Tables 13 and 14.

4.2 Bright-line abundances

In H II regions without [O III] λ4363 measurements, the bright-line method has been used to derive oxygen abundances, as the latter are usually given in terms of bright [O II] and [O III] emission lines. Pagel et al. (1979) devised the R_{23} indicator, defined by $R_{23} = [I(\text{[O II] λ3727}) + I(\text{[O III] λλ4959, 5007}\text{)}]/I(\mathrm{H}\beta)$; Skillman (1989) discussed the method further for low-metallicity galaxies. McGaugh (1991) developed a grid of photoionization models and suggested using R_{23} and an ionization proxy, represented by $O_{32} = I(\text{[O III] λλ4959, 5007}\text{)}/I(\text{[O II] λ3727}\text{)}$, to estimate oxygen abundances.[2] To break the degeneracy in the bright-line method, we have used the [N II]/[O II] ratio (e.g. McCall, Rybski & Shields 1985; McGaugh 1994; van Zee et al. 1998; Lee et al. 2003b) to choose either the 'upper branch' (high oxygen abundance) or the 'lower branch' (low oxygen abundance). In some instances, oxygen abundances with the McGaugh method could not be computed, because the R_{23} values were outside of the effective range for the models. Pilyugin (2000) proposed an empirical calibration at low metallicity with fits of oxygen abundance against bright oxygen lines. Skillman et al. (2003b) have shown that while the Pilyugin method covers a large range in R_{23}, the calibration applies mostly to H II regions with higher ionizations; see also van Zee & Haynes (2006).

Oxygen abundances derived using the bright-line calibrations are listed in Tables 13 and 14. In the absence of [O III] λ4363, oxygen abundances derived using bright-line methods are in agreement with direct abundances to within ≈0.2 dex.

5 DISCUSSION OF INDIVIDUAL GALAXIES

5.1 Cen A dwarf irregulars

Previously, Lee et al. (2003a) reported spectra for six Cen A late-type dwarf galaxies: DDO 161 (UGCA 320), ESO 324−G024,

[2] Analytical expressions for the McGaugh calibration can be found in Kobulnicky et al. (1999).

Table 4. Line ratios and properties for H II regions in Cen A dwarf irregular galaxies. Emission lines are listed in Angstroms. *F* is the observed flux ratio with respect to Hβ. *I* is the corrected intensity ratio, corrected for the adopted reddening listed, and for underlying Balmer absorption. The uncertainties in the observed line ratios account for the uncertainties in the fits to the line profiles, the surrounding continua, and the relative uncertainty in the sensitivity function listed in Table 3. Flux uncertainties in the Hβ reference line are not included. Uncertainties in the corrected line ratios account for uncertainties in the specified line and in the Hβ reference line. The reddening function, $f(\lambda)$, from equation (1) is given. Also listed are the observed Hβ flux, and the equivalent width of Hβ in emission, $EW_e(H\beta)$. Where [O III] λ4363 is measured, simultaneous solutions for the logarithmic reddening, $c(H\beta)$, from equation (1) and the equivalent width of the underlying Balmer absorption, EW_{abs} are listed. Where [O III] λ4363 is not measured, the equivalent width of the underlying Balmer absorption was set to 2 Å.

		AM 1318−444 No. 1		ESO 272−G025 No. 1		ESO 272−G025 No. 2	
Property	$f(\lambda)$	*F*	*I*	*F*	*I*	*F*	*I*
[O II] 3727	+0.325	238.2 ± 4.6	240 ± 14	199.6 ± 6.5	208 ± 13	297.8 ± 7.8	414 ± 11
[Ne III] 3869	+0.294	8.0 ± 2.1	8.0 ± 2.1	35.9 ± 3.5	36.9 ± 4.0	22.1 ± 4.3	29.5 ± 5.7
H8 + He I 3889	+0.289	10.0 ± 2.2	23.3 ± 2.5	9.8 ± 2.7	23.7 ± 3.0	...	...
Hε + He I 3970[a]	+0.269	7.5 ± 1.2	20.5 ± 1.5	...	...	...	...
H δ 4101	+0.232	13.6 ± 1.8	25.6 ± 2.0	13.1 ± 2.3	25.3 ± 2.5	...	...
H γ 4340	+0.158	39.6 ± 1.7	47.8 ± 2.1	41.7 ± 2.6	50.6 ± 2.9	32.1 ± 3.6	46.7 ± 4.0
[O III] 4363	+0.151	<3.8	<3.7	8.2 ± 2.1	7.9 ± 2.0	...	...
H β 4861	0.000	100.0 ± 3.9	100.0 ± 3.6	100.0 ± 4.0	100.0 ± 3.6	100.0 ± 4.4	100.0 ± 4.0
[O III] 4959	−0.026	70.0 ± 4.0	64.4 ± 3.7	142.7 ± 8.4	128.4 ± 7.6	55.4 ± 5.0	49.0 ± 4.4
[O III] 5007	−0.038	203.8 ± 5.1	186.9 ± 4.8	414 ± 10	370.3 ± 9.7	171.5 ± 6.4	149.3 ± 5.6
He I 5876	−0.204	5.9 ± 1.9	5.2 ± 1.7	...	...	...	...
Hα 6563	−0.299	333.1 ± 6.9	289 ± 16	342.8 ± 6.9	283 ± 15	468.3 ± 8.8	295.7 ± 5.5
[N II] 6583	−0.301	10.4 ± 5.8	8.9 ± 5.0	12.0 ± 5.5	9.6 ± 4.4	55.5 ± 7.2	34.4 ± 4.5
He I 6678	−0.314	6.1 ± 3.1	5.2 ± 2.7	...	...		
[S ii] 6716, 6731	−0.320	47.4 ± 4.4	40.3 ± 4.3	96.4 ± 8.6	76.8 ± 8.0	106.7 ± 9.0	64.7 ± 5.5
[O ii] 7320, 7330	−0.400	12.1 ± 3.5	10.1 ± 3.0	...	...	...	...
$F(H\beta)$ (ergs s^{-1} cm^{-2})		(9.19 ± 0.36) × 10^{-16}		(2.71 ± 0.11) × 10^{-16}		(2.56 ± 0.11) × 10^{-16}	
$EW_e(H\beta)$ (Å)		61.5 ± 3.6		35.4 ± 1.7		21.4 ± 1.0	
$c(H\beta)$		0.115 ± 0.074		0.179 ± 0.073		0.56	
EW_{abs} (Å)		4.9 ± 1.8		3.5 ± 1.3		2	

		ESO 274−G001 No. 1		ESO 274−G001 No. 2	ESO 274−G001 No. 3
Property	$f(\lambda)$	*F*	*I*	*F*	*F*
[O II] 3727	+0.325	253 ± 20	302 ± 24	47 ± 10	44.6 ± 6.6
H β 4861	0.000	100 ± 11	100 ± 10	...	...
[O III] 4959	−0.026	5.5 ± 7.9	5.2 ± 7.4	...	...
[O III] 5007	−0.038	39.6 ± 8.3	37.0 ± 7.8	...	...
Hα 6563	−0.299	360 ± 17	286 ± 13	100 ± 14	100.0 ± 8.1
[N II] 6583	−0.301	45 ± 14	36 ± 11	9.5 ± 11	18.0 ± 6.4
[S II] 6716	−0.319	90 ± 11	69.4 ± 8.4	...	...
[S II] 6731	−0.321	73 ± 10	56.1 ± 8.1	...	...
$F(H\beta)$ (ergs s^{-1} cm^{-2})		(3.26 ± 0.34) × 10^{-16}		(2.56 ± 0.37) × 10^{-16}[b]	(6.12 ± 0.50) × 10^{-16}[b]
$EW_e(H\beta)$ (Å)		45.8 ± 6.1		...	...
$c(H\beta)$		0.29		...	...
EW_{abs} (Å)		2		...	...

Notes: [a]Blended with [Ne III] λ3967. [b]Observed Hα flux in emission.

ESO 381−G020, ESO 383−G087, ESO 444−G084 and NGC 5264 (DDO 242). Only Hβ and Hα were detected in ESO 324−G024, and an oxygen abundance was not derived. [O III] λ4363 was detected in ESO 383−G087, and bright-line abundances were derived for the remaining four galaxies.

We briefly comment on a number of Cen A dIs. Our measured spectrum of AM 1318−444 is indicative of a metal-poor H II region, and the resulting (bright-line) oxygen abundance is about one-sixth of the solar value. While the bright-line abundance for ESO 274−G001 H II region No. 4 implies an unusually high oxygen abundance (compared to the derived lower limit), our measured intensity ratios (Table 5) suggest that the nebula is a supernova remnant; see also the discussion in Lee et al. (2006a). If the object in question is a supernova remnant, the measured I([N II] λ6583)/I(Hα), I([S II] λ6731)/I(Hα) and the model grid from Dopita et al. (1984, their fig. 8) yield an estimate of 12 + log(O/H) $\simeq$ 7.8 ± 0.1 for the oxygen abundance. As an edge-on dwarf galaxy, ESO 274−G001 is reminiscent of NGC 55 in the Sculptor group and NGC 1560 in the IC 342 group. These galaxies may provide further opportunities to investigate the possibility of abundance gradients in low-luminosity late-type galaxies. In fact, Lee et al. (2003a) reported an unusually high (bright-line) abundance for NGC 5264 in the Cen A group. Additional high signal-to-noise spectra would be valuable in confirming this result. For ESO 324−G024, we obtained a higher quality spectrum compared to the observation described in Lee et al. (2003a), but we did not detect [O III] λ4363. The bright-line oxygen abundance derived for ESO 381−G020 is 0.12 dex higher than the bright-line value determined in Lee et al. (2003a), but these values are well within the acceptable uncertainty ($\sim$0.2 dex) associated with bright-line abundances. In all, the derived oxygen abundances

Table 5. Line ratios and properties for H II regions in Cen A dwarf irregular galaxies (continued). See Table 4 for comments.

Property	$f(\lambda)$	ESO 274−G001 No. 4		ESO 274−G001 No. 5		ESO 274−G001 No. 6	
		F	*I*	*F*	*I*	*F*	*I*
[O II] 3727	+0.325	200.4 ± 3.2	373 ± 15	129 ± 35	139 ± 38	446 ± 23	605 ± 31
[Ne III] 3869	+0.294	21.3 ± 2.7	36.9 ± 4.8	...	...	...	...
[S II] 4068	+0.241	23.1 ± 2.7	35.7 ± 4.3	...	...	...	...
Hδ 4101	+0.232	7.3 ± 2.1	26.0 ± 3.3	...	...	...	...
Hγ 4340	+0.158	32.4 ± 2.1	53.6 ± 2.9	...	...	48.7 ± 9.4	59 ± 11
[O III] 4363	+0.151	<5.8	<7.3	...	...	...	...
Hβ 4861	0.000	100.0 ± 3.4	100.0 ± 3.1	100 ± 33	100 ± 27	100 ± 10	100.0 ± 9.8
[O III] 4959	−0.026	97.8 ± 5.2	83.5 ± 4.4	170 ± 33	134 ± 26	33.8 ± 8.9	31.6 ± 8.3
[O III] 5007	−0.038	296.0 ± 6.5	246.1 ± 5.5	506 ± 43	397 ± 34	126 ± 11	116 ± 10
[O I] 6300 + [S III] 6312	−0.264	157.9 ± 6.5	79.2 ± 4.0	...	...	...	...
[O I] 6363	−0.272	97.3 ± 9.7	23.1 ± 2.5	...	...	...	...
Hα 6563	−0.299	625 ± 12	297 ± 11	434 ± 48	286 ± 30	405 ± 17	286 ± 12
[N II] 6583	−0.301	97.3 ± 9.7	45.0 ± 4.7	...	...	68 ± 14	47.6 ± 9.7
[S II] 6716	−0.319	120.2 ± 3.2	53.5 ± 2.4	...	...	117 ± 12[a]	80.0 ± 8.0
[S II] 6731	−0.321	110.5 ± 3.2	49.0 ± 2.3	...	...	117 ± 12[a]	80.0 ± 8.0
[Ar III] 7136	−0.375	54.1 ± 5.6	21.3 ± 2.4	...	...	...	...
[O II] 7320, 7330	−0.400	143.3 ± 7.5	53.2 ± 3.7	...	...	...	...
F(Hβ) (ergs s^{-1} cm^{-2})		(1.971 ± 0.068) × 10^{-15}		(8.6 ± 2.8) × 10^{-17}		(2.77 ± 0.28) × 10^{-16}	
EW$_e$(Hβ) (Å)		16.69 ± 0.60		8.6 ± 2.8		48.6 ± 6.5	
c(Hβ)		0.965 ± 0.048		0.38		0.46	
EW$_{abs}$ (Å)		1.75 ± 0.49		2		2	

Property	$f(\lambda)$	ESO 274−G001 No. 7		ESO 274−G001 No. 8		ESO 324−G024 No. 1	
		F	*I*	*F*	*I*	*F*	*I*
[O II] 3727	+0.325	366 ± 15	513 ± 21	268 ± 38	287 ± 41	357.8 ± 9.4	429 ± 11
Hγ 4340	+0.158	46.0 ± 6.7	56.0 ± 7.8	...	...	40.2 ± 3.5	48.9 ± 3.7
Hβ 4861	0.000	100.0 ± 8.3	100.0 ± 8.2	100 ± 19	100 ± 16	100.0 ± 4.6	100.0 ± 4.4
[O III] 4959	−0.026	43.4 ± 6.2	41.6 ± 5.9	...	...	63.1 ± 5.3	58.9 ± 4.9
[O III] 5007	−0.038	96.3 ± 6.5	91.2 ± 6.2	55 ± 15	47 ± 13	162.5 ± 6.6	150.3 ± 6.1
Hα 6563	−0.299	401 ± 10	286.9 ± 7.4	383 ± 27	286 ± 20	370.7 ± 9.7	287.3 ± 7.4
[N II] 6583	−0.301	62.9 ± 8.4	44.8 ± 6.0	36 ± 21	26 ± 16	19.4 ± 8.1	14.9 ± 6.2
[S II] 6716	−0.319	109 ± 12	76.2 ± 8.4	...	...	46.0 ± 5.8[a]	34.8 ± 4.4
[S II] 6731	−0.321	48 ± 11	33.6 ± 7.4	...	...	46.0 ± 5.8[a]	34.8 ± 4.4
F(Hβ) (ergs s^{-1} cm^{-2})		(3.97 ± 0.33) × 10^{-16}		(1.32 ± 0.25) × 10^{-16}		(4.14 ± 0.19) × 10^{-16}	
EW$_e$(Hβ) (Å)		148 ± 32		14.1 ± 2.7		38.5 ± 2.1	
c(Hβ)		0.47		0.27		0.31	
EW$_{abs}$ (Å)		2		2		2	

Note: [a][S II] lines unresolved.

for the present sample of Cen A dIs (cf. Table 1) are in the range between about 10 to 50 per cent of the solar value, which are in general agreement with the results obtained by Webster & Smith (1983) and Webster et al. (1983).

5.2 Nearby dwarf irregulars

5.2.1 DDO 47

Skillman, Kennicutt & Hodge (1989) obtained spectra for the H II region SHK91 No. 18 in DDO 47 using the IIDS spectrometer on the KPNO 2.1-m telescope. With their [O III] λ4363 measurement, they derived an oxygen abundance of 12 + log (O/H) = 7.89 ± 0.20. In our spectrum, we measured [O III] λ4363 and derived an oxygen abundance of 12 + log (O/H) = 7.92 ± 0.06, in agreement with Skillman et al. (1989). We have also measured He II λ4686 Å. As He II emission is indicative of the presence of O^{+3}, the latter is generally a small contributor to the total oxygen abundance. For example, Kennicutt & Skillman (1993) measured He II emission in I Zw 18 and found that the resulting O^{+3} contribution was of order 1 to 4 per cent. In H II region SHK91 No. 18, the He II 4686 Å to Hβ flux ratio is about 10 per cent, which implies that the resulting contribution by O^{+3} to the total oxygen abundance could be of order 10 per cent. For comparison with other dIs, we have not included any O^{+3} contribution in the total oxygen abundance for DDO 47.

5.2.2 NGC 3109

The optical appearance (e.g. Carignan 1985; Jobin & Carignan 1990) is suggestive of a low-luminosity spiral galaxy. From the data reported previously by Lee et al. (2003a), the authors suggested the presence of an abundance gradient in NGC 3109, which had been previously hinted by Grebel (2001a,b). We did not measure [O III] λ4363 in any of the spectra shown here. The subsequent mean of six bright-line abundances is 7.94 ± 0.2, which is larger than the Lee et al. (2003b) value by about 0.2 dex, but is in better

Table 6. Line ratios and properties for H II regions in Cen A dwarf irregular galaxies (continued). See Table 4 for comments.

Property	$f(\lambda)$	ESO 324−G024 No. 2		ESO 324−G024 No. 3		ESO 324−G024 No. 4	
		F	I	F	I	F	I
[O II] 3727	+0.325	334 ± 10	375 ± 12	338 ± 11	377 ± 12	144.7 ± 3.1	152.6 ± 7.6
H11 3772	+0.316	...	...	...	...	3.4 ± 2.4	7.4 ± 2.6
H10 3799	+0.310	...	...	...	...	5.8 ± 2.7	10.9 ± 2.9
H9 3835	+0.302	...	...	...	...	4.7 ± 1.9	11.0 ± 2.0
[Ne III] 3869	+0.294	...	...	...	...	22.3 ± 2.0	23.3 ± 2.3
H8 + He I 3889	+0.289	...	...	...	...	21.6 ± 2.0	29.2 ± 2.4
Hε + He I 3970[a]	+0.269	...	...	...	...	14.4 ± 1.8	21.6 ± 2.0
Hδ 4101	+0.232	...	...	...	...	19.1 ±1.8	25.5 ± 2.0
Hγ 4340	+0.158	40.6 ± 5.8	46.8 ± 6.0	43.7 ± 5.3	48.8 ± 5.5	44.5 ± 1.6	49.2 ± 1.9
[O III] 4363	+ 0.151	...	...	...	...	5.3 ± 1.3	5.3 ± 1.3
Hβ 4861	0.000	100.0 ± 6.0	100.0 ± 5.8	100.0 ± 7.6	100.0 ± 7.4	100.0 ± 3.1	100.0 ± 3.0
[O III] 4959	−0.026	27.6 ± 5.5	26.1 ± 5.2	25.8 ± 6.8	24.9 ± 6.6	129.6 ± 8.1	124.8 ± 7.8
[O III] 5007	−0.038	80.5 ± 7.0	75.8 ± 6.6	98.4 ± 9.2	94.5 ± 8.8	373 ± 10	358 ± 10
He I 5876	−0.204	...	...	...	...	8.3 ± 1.0	7.63 ± 0.94
Hα 6563	−0.299	336 ±10	283.3 ± 8.6	331 ± 12	287 ± 10	316.0 ± 8.3	285 ± 14
[N II] 6583	−0.301	7.5 ± 8.3	6.2 ± 6.9	17.4 ± 9.2	15.0 ± 7.9	3.1 ± 1.4	2.8 ± 1.3
He I 6678	−0.314	...	...	...	...	5.8 ± 1.9	5.2 ± 1.7
[S II] 6716, 6731	−0.320	77 ± 12	63.5 ± 9.9	39.4 ± 4.9	33.7 ± 4.2	15.5 ± 2.5	13.8 ± 2.3
[Ar III] 7136	−0.375	...	...	...	...	8.5 ± 1.6	7.5 ± 1.5
$F(H\beta)$ (ergs s^{-1} cm^{-2})		(2.91 ± 0.17) × 10^{-16}		(2.32 ± 0.18) × 10^{-16}		(1.070 ± 0.033) × 10^{-15}	
$EW_e(H\beta)$ (Å)		46.9 ± 3.7		81 ± 11		164 ± 16	
$c(H\beta)$		0.21		0.18		0.112 ± 0.060	
EW_{abs} (Å)		2		2		5.1 ± 2.8	

Property	$f(\lambda)$	ESO 324−G024 No. 5		ESO 325−G011 No. 1		ESO 325−G011 No. 2	
		F	I	F	I	F	I
[O II] 3727	+0.325	164.9 ± 3.4	174.1 ± 8.8	338 ± 32	358 ± 34	246.1 ± 8.7	234.4 ± 8.3
H 11 3772	+0.316	4.2 ± 2.6	8.4 ± 2.8	...	...	...	...
H 10 3799	+0.310	5.9 ± 2.9	11.3 ± 3.1	...	...	...	...
H 9 3835	+0.302	4.3 ± 1.8	10.8 ± 1.9	...	...	...	...
[Ne III] 3869	+0.294	23.1 ± 1.9	24.2 ± 2.2	...	...	...	...
H8 + He I 3889	+0.289	21.2 ± 1.9	29.2 ± 2.3	...	...	...	...
Hε + He I 3970[a]	+0.269	15.0 ± 1.9	22.3 ± 2.2	...	...	...	...
Hδ 4101	+0.232	19.3 ± 1.8	25.7 ± 2.0	...	...	...	...
Hγ 4340	+0.158	44.2 ± 1.9	49.0 ± 2.2	...	...	40.3 ± 5.4	43.7 ± 5.1
[O III] 4363	+0.151	4.4 ± 1.5	4.4 ± 1.5	...	...	...	...
Hβ 4861	0.000	100.0 ± 3.1	100.0 ± 3.0	100 ± 16	100 ± 16	100.0 ± 6.1	100.0 ± 5.8
[O III] 4959	−0.026	128.7 ± 8.0	123.9 ± 7.7	19 ± 12	18 ± 12	92.9 ± 6.7	87.8 ± 6.3
[O III] 5007	−0.038	373 ± 10	357.7 ± 9.9	43 ± 13	41 ± 12	261.5 ± 8.1	247.0 ± 7.7
He I 5876	−0.204	7.8 ± 1.3	7.2 ± 1.2	...	...	...	...
Hα 6563	−0.299	317.1 ± 8.0	285 ± 14	323 ± 17	286 ± 15	294.3 ± 8.9	281.6 ± 8.4
[N II] 6583	−0.301	4.3 ± 1.5	3.9 ± 1.4	14 ± 14	12 ± 12	7.0 ± 7.0	6.6 ± 6.6
He I 6678	−0.314	9.7 ± 2.5	8.7 ± 2.3	...	...	...	...
[S II] 6716, 6731	−0.320	15.5 ± 2.8	13.8 ± 2.6	...	...	34.2 ± 6.8	32.1 ± 6.4
[Ar III] 7136	−0.375	9.3 ± 1.6	8.2 ± 1.5	...	...	...	...
$F(H\beta)$ (ergs s^{-1} cm^{-2})		(1.270 ± 0.039) × 10^{-15}		(1.34 ± 0.22) × 10^{-16}		(3.57 ± 0.22) × 10^{-16}	
$EW_e(H\beta)$ (Å)		173 ± 18		51 ± 11		34.6 ± 2.5	
$c(H\beta)$		0.113 ± 0.061		0.13		0	
EW_{abs} (Å)		5.4 ± 3.1		2		2	

Note: [a]Blended with [Ne III] λ3967.

agreement with other dwarfs at comparable optical luminosity. Since this galaxy is known to contain multiple H II regions and planetary nebulae (i.e. Bresolin, Capaccioli & Piotto 1993; Peña, Richer & Stasińska 2006), deep spectra of these nebulae would be valuable to confirm the presence or absence of a radial gradient in oxygen abundance.

5.2.3 *Sextans B*

Published nebular abundances for Sextans B have differed by as much as 0.5 dex. Stasińska, Comte & Vigroux (1986) published a limit of $12 + \log(O/H) > 7.38$ from data obtained with the IIDS detector on the ESO 3.6-m telescope. Skillman et al. (1989) reported

Table 7. Line ratios and properties for H II regions in Cen A dwarf irregular galaxies (continued). See Table 4 for comments.

		ESO 325−G011 No. 3		ESO 325−G011 No. 4		ESO 325−G011 No. 5[a]	
Property	$f(\lambda)$	F	I	F	I	F	I
[O II] 3727	+0.325	307 ± 29	311 ± 30	200.7 ± 5.5	217.6 ± 6.0	166 ± 13	309 ± 24
Hδ 4101	+0.232	...	...	21.0 ± 3.4	24.5 ± 3.6	...	...
Hγ 4340	+0.158	...	...	38.7 ± 2.9	41.9 ± 3.0	...	...
[O III] 4363	+0.151	...	...	< 8.4	< 8.6	...	...
Hβ 4861	0.000	100 ± 13	100 ± 12	100.0 ± 3.4	100.0 ± 3.3	100.0 ± 7.5	100.0 ± 4.2
[O III] 4959	−0.026	39 ± 11	39 ± 11	80.7 ± 5.9	78.8 ± 5.8	36.6 ± 7.5	18.8 ± 3.9
[O III] 5007	−0.038	118 ± 13	116 ± 13	244.7 ± 7.4	238.0 ± 7.2	66.7 ± 9.0	32.8 ± 4.4
He I 5876	−0.204	...	...	12.2 ± 2.7	11.3 ± 2.5	...	...
Hα 6563	−0.299	296 ± 23	286 ± 22	318.2 ± 7.4	287.0 ± 6.7	1440 ± 25	286.8 ± 4.8
[N II] 6583	−0.301	...	...	2.8 ± 5.9	2.5 ± 5.3	556 ± 23	104.0 ± 4.2
[S II] 6716	−0.319	...	...	16.9 ± 3.5[b]	15.1 ± 3.1	119 ± 13	20.9 ± 2.3
[S II] 6731	−0.321	...	...	16.9 ± 3.5[b]	15.1 ± 3.1	133 ± 13	23.1 ± 2.3
F(Hβ) (ergs s^{-1} cm^{-2})		(1.67 ± 0.21) × 10^{-16}		(8.75 ± 0.30) × 10^{-16}		(4.54 ± 0.34) × 10^{-16}	
EW$_e$(Hβ) (Å)		121 ± 39		121 ± 10		2.64 ± 0.20	
c(Hβ)		0.04		0.13		1.6	
EW$_{abs}$ (Å)		2		2		2	

		ESO 381−G020 No. 1		ESO 381−G020 No. 2		ESO 381−G020 No. 3	
Property	$f(\lambda)$	F	I	F	I	F	I
[O II] 3727	+0.325	176.1 ± 8.3	187.8 ± 8.9	328 ± 64	475 ± 92	202.3 ± 5.5	202.3 ± 5.5
[Ne III] 3869	+0.294	28.4 ± 5.6	29.9 ± 5.9	...	...	23.7 ± 5.3	23.7 ± 5.3
Hε + He I 3970[c]	+0.269	...	...	...	...	18.9 ± 3.3	18.9 ± 3.3
Hδ 4101	+0.232	...	...	...	...	15.3 ± 3.2	15.3 ± 3.2
Hγ 4340	+0.158	44.6 ± 4.5	52.0 ± 4.5	...	...	38.4 ± 3.4	38.4 ± 3.4
[O III] 4363	+ 0.151	<16.4	<16.3	...	...	<8.0	<8.0
Hβ 4861	0.000	100.0 ± 4.1	100.0 ± 3.8	100 ± 38	100 ± 31	100.0 ± 4.5	100.0 ± 4.5
[O III] 4959	−0.026	131.2 ± 8.7	122.0 ± 8.1	152 ± 38	116 ± 27	90.7 ± 6.5	90.7 ± 6.5
[O III] 5007	−0.038	384 ± 11	356 ± 10	335 ± 52	251 ± 39	258.7 ± 8.1	258.7 ± 8.1
He I 5876	−0.204	...	...	...	...	11.2 ± 2.2	11.2 ± 2.2
Hα 6563	−0.299	340.7 ± 8.7	287.3 ± 7.3	604 ± 44	286 ± 20	271.4 ± 6.7	271.4 ± 6.7
[N II] 6583	−0.301	3.6 ± 6.9	3.0 ± 5.8	38 ± 35	18 ± 16	0.4 ± 5.4	0.4 ± 5.4
[S II] 6716, 6731	−0.320	48.6 ± 8.4	40.3 ± 7.0	...	...	24.3 ± 3.3	24.3 ± 3.3
F(Hβ) (ergs s^{-1} cm^{-2})		(8.28 ± 0.34) × 10^{-16}		(1.00 ± 0.38) × 10^{-16}		(1.567 ± 0.071) × 10^{-15}	
EW$_e$(Hβ) (Å)		30.8 ± 1.5		8.1 ± 3.1		53.4 ± 3.3	
c(Hβ)		0.17		0.79		0	
EW$_{abs}$ (Å)		2		2		0	

Notes: [a]Background galaxy with $v_\odot \approx 26200$ km s^{-1}. [b][S II] unresolved. [c]Blended with [Ne III] λ3967.

a higher lower limit to the oxygen abundance: 12 + log (O/H) > 7.56. From data obtained with the IDS on the 2.5-m INT telescope, Moles, Aparicio & Masegosa (1990) measured [O III] λ4363 and subsequently derived an oxygen abundance 12 + log(O/H) = 8.11. If the higher value is adopted, the present-day metallicity appears ∼0.3 dex too high for its galaxy optical luminosity, compared to other dwarf irregulars at comparable luminosity.

Kniazev et al. (2005) reported NTT spectra for one planetary nebula and six H II regions in Sextans B, from which [O III] λ4363 was detected in the planetary nebula and in three H II regions. They reported [O III] λ4363 in SHK91 No. 5, but their spectrum is cut-off below about 3800 Å, and there is no measured [O II] λ3727. Alternatively, they used their [O II] λλ7320, 7330 measurement to derive the O^+/H abundance with the method developed to derive oxygen abundances for metal-poor galaxies observed in the Sloan Digital Sky Survey (Kniazev et al. 2004). Their resulting oxygen abundance for H II region No. 5 is 12 + log (O/H) = 7.84 ± 0.05. Kniazev et al. (2005) claimed that the recent chemical enrichment was spatially inhomogeneous over length scales as large as 1 kpc, based on a dispersion of 0.31 dex for direct abundances in three H II regions. With FORS2 on Very Large Telescope (VLT), Magrini et al. (2005) measured spectra of H II regions and planetary nebulae, and detected [O III] λ4363 in three H II regions, including No. 5. Their direct oxygen abundance is 12 + log (O/H) = 7.69 ± 0.14, which agrees with the Kniazev et al. (2005) result.

We measured [O III] λ4363 only in H II region No. 5, but our spectrum includes the full range of optical emission lines from [O II] λ3727 to [S II] λλ6716, 6731 (Fig 3 and Table 12). Our resulting direct abundance is 12 + log (O/H) = 7.80 ± 0.13, which also agrees with the values reported by Kniazev et al. (2005) and Magrini et al. (2005). The data presented here shows that the derived bright-line abundances for H II regions SHK91 Nos. 1, 2, 5 and 10 all agree to within ≈0.1 dex (14). Although the direct abundance for SHK91 No. 5 and the bright-line abundance for SHK91 No. 10 differ by 0.25 dex, the difference is comparable to our adopted uncertainty of 0.2 dex for a bright-line abundance.

Table 8. Line ratios and properties for H II regions in Cen A dwarf irregular galaxies (continued). See Table 4 for comments.

		ESO 381−G020 No. 4		ESO 381−G020 No. 5		ESO 381−G020 No. 6	
Property	$f(\lambda)$	F	I	F	I	F	I
[O II] 3727	+0.325	320 ± 30	422 ± 39	74.9 ± 7.9	74.9 ± 7.9	108 ± 18	108 ± 18
Hδ 4101	+0.232	...	...	12.7 ± 3.7	12.7 ± 3.7	...	...
Hγ 4340	+0.158	...	...	43.8 ± 4.3	43.8 ± 4.3	33.4 ± 8.0	33.4 ± 8.0
Hβ 4861	0.000	100 ± 14	100 ± 13	100.0 ± 3.9	100.0 ± 3.9	100 ± 11	100 ± 11
[O III] 4959	−0.026	30 ± 11	26.8 ± 9.8	70.4 ± 4.8	70.4 ± 4.8	51.0 ± 9.6	51.0 ± 9.6
[O III] 5007	−0.038	52 ± 11	45.5 ± 9.6	199.5 ± 6.1	199.5 ± 6.1	137 ± 12	137 ± 12
Hα 6563	−0.299	438 ± 18	285 ± 11	270.6 ± 5.9	270.6 ± 5.9	277 ± 13	277 ± 13
[N II] 6583	−0.301	...	...	5.8 ± 4.8	5.8 ± 4.8	...	...
F(Hβ) (ergs s^{-1} cm^{-2})		(2.27 ± 0.32) × 10^{-16}		(8.62 ± 0.34) × 10^{-16}		(2.96 ± 0.32) × 10^{-16}	
EW$_e$(Hβ) (Å)		19.8 ± 2.9		330 ± 76		289 ± 165	
c(Hβ)		0.5		0		0	
EW$_{abs}$ (Å)		2		0		0	

		IC 4247 No. 1		IC 4247 No. 2	
Property	$f(\lambda)$	F	I	F	I
[O II] 3727	+0.325	404.1 ± 8.2	410.2 ± 8.3	577 ± 12	523 ± 11
[Ne III] 3869	+0.294	50.9 ± 7.2	51.6 ± 7.3	...	...
Hγ 4340	+0.158	33.4 ± 3.3	33.6 ± 3.3	...	...
Hβ 4861	0.000	100.0 ± 5.1	100.0 ± 5.1	100.0 ± 7.0	100.0 ± 6.2
[O III] 4959	−0.026	95.3 ± 7.1	95.2 ± 7.1	26.2 ± 4.9	23.2 ± 4.3
[O III] 5007	−0.038	292.3 ± 9.0	291.8 ± 9.0	83.4 ± 6.2	73.6 ± 5.5
Hα 6563	−0.299	291.2 ± 7.4	287.2 ± 7.3	322 ± 12	286 ± 10
[N II] 6583	−0.301	9.1 ± 5.9	9.0 ± 5.8	11.9 ± 9.3	10.3 ± 8.1
[S II] 6716, 6731	−0.320	41.7 ± 6.1	41.1 ± 6.0	28.3 ± 4.4	24.5 ± 3.8
F(Hβ) (ergs s^{-1} cm^{-2})		(7.33 ± 0.38) × 10^{-16}		(4.85 ± 0.34) × 10^{-16}	
EW$_e$(Hβ) (Å)		15.40 ± 0.83		10.75 ± 0.77	
c(Hβ)		0.02		0.03	
EW$_{abs}$ (Å)		0		1.4	

6 EXPLORATION OF ENVIRONMENTAL EFFECTS

If dwarf galaxies are more robust to the effects of internal processes, such as supernova feedback, external processes found within environments of galaxy groups may be more damaging to the 'health' of gas-rich dwarf galaxies. Galaxy–galaxy encounters create tidal interactions, which can remove stellar and/or gaseous material and eject the stripped material into the intragroup medium. Disturbed galaxy morphologies are also indicative of these interactions. Groups may contain hot ($T \sim 10^7$ K) dense X-ray emitting gas, which could provide an agent for ram-pressure stripping, if group galaxies traverse the intragroup medium at high speeds. However, only the highest mass groups have significant X-ray luminosities (see, e.g. Mulchaey 2000). In most nearby groups (at least within the Local Volume), it is difficult to measure strong X-ray emission. Bouchard et al. (2007) have suggested that ram-pressure stripping may have been responsible to explain the lower H I content in Cen A dwarfs relative to dwarfs in the Local Group and the Scl group. At present, we assume that the presence of X-ray gas is negligible, although the possibility of warm gas ($T \sim 10^6$ K) is not entirely ruled out (Mulchaey 2000). Higher star formation rates can also be induced by tidal interactions, as molecular gas is subsequently compressed and shock heated. A subsequent result would be a larger fraction of galaxies with strong emission lines and/or blue colours in these environments. Unfortunately, extensive galaxy surface photometry has not yet been obtained for Cen A or Sculptor (Scl) group dwarf galaxies, although narrow-band Hα images have been obtained for some of the dIs in the two groups (Skillman, Côté & Miller 2003a; S. Côté, personal communication). Although we cannot yet compare the star formation properties, we can compare the end results to their present-day chemical evolution. In the discussion which follows, we have also included additional spectra for Cen A dwarfs from Lee et al. (2003a) and Scl group dwarfs from Skillman et al. (2003b). We have adopted a distance of 3.0 Mpc for the Scl group dwarfs AM0106−382 and ESO348−G009.

6.1 Luminosity–metallicity relation

The optical luminosity–metallicity relation has long been used as a diagnostic for the evolution of nearby star-forming dIs; e.g. Skillman et al. (1989), Richer & McCall (1995), Lee et al. (2003b), van Zee & Haynes (2006). To augment the local sample described by Lee et al. (2003b), additional galaxies with [O III] λ4363 measurements and/or distances from stellar indicators are taken from the literature: DDO 167 (Skillman et al. 1989; Karachentsev et al. 2003b), ESO 489−G056 (Rönnback & Bergvall 1995; Karachentsev et al. 2002c), NGC 1705 (Lee & Skillman 2004), NGC 3738 (Martin 1997; Karachentsev et al. 2003a), NGC 4449 (Martin 1997; Karachentsev et al. 2003a), NGC 6822 (Lee et al. 2006a) and WLM (Lee et al. 2005). We have also included direct and bright-line abundances for additional Cen A and Scl group dwarf irregulars from Lee et al. (2003a) and Skillman et al. (2003b).

The luminosity–metallicity relation is shown in Fig. 6(a). The solid line is a fit to the sample of nearby dwarfs as described above. Cen A and Scl group dwarfs with [O III] λ4363 measurements are in

Table 9. Line ratios and properties for H II regions in the Cen A dwarf galaxy IC 4316. See Table 4 for comments.

		IC 4316 No. 1		IC 4316 No. 2		IC 4316 No. 3	
Property	$f(\lambda)$	F	I	F	I	F	I
[O II] 3727	+0.325	415.4 ± 9.8	541 ± 13	305.1 ± 3.8	305.1 ± 3.8	484 ± 13	510 ± 13
H 9 3835	+0.302	...	...	2.2 ± 1.1	2.2 ± 1.1	...	...
[Ne III] 3869	+0.294	...	...	21.3 ± 1.2	21.3 ± 1.2	48 ± 10	49 ± 11
H8 + He I 3889	+0.289	...	...	18.0 ± 1.2	18.0 ± 1.2	...	...
Hε + He I 3970[a]	+0.269	...	...	19.2 ± 1.2	19.2 ± 1.2	...	...
Hδ 4101	+0.232	...	...	22.3 ± 1.2	22.3 ± 1.2	...	...
Hγ 4340	+0.158	37.1 ± 3.3	50.6 ± 3.6	44.11 ± 0.97	44.11 ± 0.97	...	...
[O III] 4363	+0.151	...	...	<2.3	<2.3	...	...
He I 4471	+0.116	...	...	3.06 ± 0.62	3.06 ± 0.62	...	...
Hβ 4861	0.000	100.0 ± 5.2	100.0 ± 4.8	100.0 ± 3.9	100.0 ± 3.9	100.0 ± 6.8	100.0 ± 6.0
[O III] 4959	−0.026	30.1 ± 4.0	27.0 ± 3.6	90.2 ± 6.5	90.2 ± 6.5	92.3 ± 6.7	80.8 ± 5.9
[O III] 5007	−0.038	59.6 ± 4.8	52.9 ± 4.3	245.6 ± 7.8	245.6 ± 7.8	294.2 ± 8.5	255.9 ± 7.4
He I 5876	−0.204	...	...	9.46 ± 0.98	9.46 ± 0.98	...	...
[O I] 6300 + [S III] 6312	−0.265	...	...	7.0 ± 1.3	7.0 ± 1.3	...	...
Hα 6563	−0.299	418 ± 12	285.2 ± 8.3	258.4 ± 6.3	258.4 ± 6.3	368.8 ± 9.8	286.1 ± 7.4
[N II] 6583	−0.301	45 ± 10	30.4 ± 6.7	26.9 ± 4.9	26.9 ± 4.9	46.7 ± 7.8	35.3 ± 5.9
He I 6678	−0.314	...	...	4.0 ± 1.0	4.0 ± 1.0	...	...
[S II] 6716	−0.319	175 ± 12[b]	114.9 ± 7.7	26.2 ± 1.1	26.2 ± 1.1	148 ± 13[b]	110.7 ± 9.7
[S II] 6731	−0.321	175 ± 12[b]	114.9 ± 7.7	22.0 ± 1.1	22.0 ± 1.1	148 ± 13[b]	110.7 ± 9.7
[Ar III] 7136	−0.375	...	...	10.08 ± 0.97	10.08 ± 0.97	...	...
$F(\mathrm{H}\beta)$ (ergs s^{-1} cm^{-2})		(2.44 ± 0.13) × 10^{-16}		(1.330 ± 0.052) × 10^{-15}		(1.291 ± 0.088) × 10^{-16}	
$\mathrm{EW_e}(\mathrm{H}\beta)$ (Å)		24.1 ± 1.4		83.1 ± 6.6		15.8 ± 1.1	
$c(\mathrm{H}\beta)$		0.46		0		0.23	
$\mathrm{EW_{abs}}$ (Å)		2		0		2	

		IC 4316 No. 4		IC 4316 No. 5		IC 4316 No. 6	
Property	$f(\lambda)$	F	I	F	I	F	I
[O II] 3727	+0.325	338.3 ± 8.3	375.8 ± 9.2	352.6 ± 5.9	395.1 ± 6.6	328.6 ± 5.2	366.2 ± 5.8
[Ne III] 3869	+0.294	...	...	12.5 ± 2.6	13.8 ± 2.9	9.6 ± 1.9	10.6 ± 2.1
H8 + He I 3889	+0.289	...	...	...	...	7.8 ± 2.4	14.7 ± 2.6
Hε + He I 3970[a]	+0.269	...	...	...	...	8.9 ± 2.1	15.4 ± 2.3
Hδ 4101	+0.232	...	...	11.3 ± 1.6	20.1 ± 1.7	13.9 ± 1.8	20.4 ± 1.9
Hγ 4340	+0.158	31.8 ± 3.1	40.5 ± 3.2	37.8 ± 2.1	45.3 ± 2.1	39.5 ± 2.2	45.3 ± 2.3
Hβ 4861	0.000	100.0 ± 4.3	100.0 ± 4.0	100.0 ± 3.1	100.0 ± 2.9	100.0 ± 3.8	100.0 ± 3.7
[O III] 4959	−0.026	46.8 ± 4.4	43.2 ± 4.1	54.6 ± 3.7	51.2 ± 3.5	56.8 ± 3.8	54.3 ± 3.6
[O III] 5007	−0.038	138.6 ± 5.5	127.0 ± 5.0	150.2 ± 4.6	140.0 ± 4.3	161.1 ± 4.7	153.2 ± 4.5
He I 5876	−0.204	...	...	7.9 ± 1.7	6.8 ± 1.5	7.7 ± 2.2	6.8 ± 1.9
Hα 6563	−0.299	353.5 ± 8.6	286.1 ± 6.7	344.3 ± 7.0	284.1 ± 5.7	334.4 ± 6.2	285.6 ± 5.3
[N II] 6583	−0.301	28.3 ± 6.9	22.5 ± 5.5	30.7 ± 5.6	25.0 ± 4.6	29.9 ± 4.9	25.3 ± 4.2
[S II] 6716, 6731	−0.320	86.6 ± 5.6	68.3 ± 4.4	80.9 ± 3.6	65.3 ± 2.9	70.5 ± 4.9	59.3 ± 4.1
$F(\mathrm{H}\beta)$ (ergs s^{-1} cm^{-2})		(3.09 ± 0.13) × 10^{-16}		(9.26 ± 0.29) × 10^{-16}		(4.82 ± 0.18) × 10^{-16}	
$\mathrm{EW_e}(\mathrm{H}\beta)$ (Å)		28.8 ± 1.4		38.2 ± 1.5		58.1 ± 3.4	
$c(\mathrm{H}\beta)$		0.23		0.22		0.19	
$\mathrm{EW_{abs}}$ (Å)		2		2		2	

Notes: [a]Blended with [Ne III] λ3967. [b][S II] unresolved.

best agreement with the fit and with the locus of nearby dwarfs that have [O III] λ4363 measurements. Although the spectra for NGC 5264 are of lower signal-to-noise, this galaxy exhibits unusually high oxygen abundance for its luminosity, which suggests a more spiral-like nature to the galaxy and warrants future measurements. Three Cen A dwarfs with [O III] λ4363 detections have oxygen abundances consistent for their optical luminosities. For the other Cen A dIs without [O III] λ4363 measurements, their oxygen abundances generally appear higher than abundances for nearby dIs at similar luminosities. We have found that [O III] λ4363 oxygen abundances exhibit the least dispersion in the luminosity–metallicity relationship, and there is no apparent difference between dIs in Cen A and Scl groups.[3] It would be interesting to examine the relative dispersion in the luminosity–metallicity relation at near-infrared wavelengths; see Lee et al. (2006b) and references within.

6.2 Gas fraction–metallicity relation

The gas content in galaxies may be sensitive to environmental effects, and we examine here how environment may affect chemical

[3] From observations of Virgo cluster dIs, Lee et al. (2003c) showed that the cluster environment appears to have little effect on the optical luminosity–metallicity relation.

Table 10. Line ratios and properties for H II regions in DDO 47. SHK91: Strobel et al. (1991). See Table 4 for additional comments, and Fig. 2 for location of H II regions.

		SHK91 No. 16[a]		SHK91 No. 17		SHK91 No. 18[b]	
Property	$f(\lambda)$	F	I	F	I	F	I
[O II] 3727	+0.325	246.7 ± 6.5	244.6 ± 6.4	245 ± 11	245 ± 11	67.5 ± 4.3	64.6 ± 4.1
[Ne III] 3869	+0.294	...	...	34.9 ± 7.0	34.9 ± 7.0	36.7 ± 3.6	35.1 ± 3.4
Hε + He I 3970[c]	+0.269	...	...	...	...	23.0 ± 2.6	28.3 ± 2.5
Hδ 4101	+0.232	...	...	...	...	19.5 ± 1.9	24.8 ± 1.8
Hγ 4340	+0.158	34.9 ± 3.0	37.4 ± 3.0	42.4 ± 5.4	42.4 ± 5.4	41.1 ± 1.9	44.5 ± 1.8
[O III] 4363	+0.151	...	...	...	...	9.7 ± 1.5	9.3 ± 1.4
[He II] 4686	+0.050	...	...	...	...	11.1 ± 2.0	10.6 ± 1.9
Hβ 4861	0.000	100.0 ± 3.8	100.0 ± 3.7	100.0 ± 7.0	100.0 ± 7.0	100.0 ± 3.4	100.0 ± 3.3
[O III] 4959	−0.026	55.9 ± 4.0	54.5 ± 3.9	133 ± 10	133 ± 10	205 ± 12	196 ± 12
[O III] 5007	−0.038	175.9 ± 5.0	171.5 ± 4.9	404 ± 13	404 ± 13	594 ± 15	568 ± 14
He I 5876	−0.204	...	...	9.6 ± 4.5	9.6 ± 4.5	7.4 ± 1.5	7.1 ± 1.4
Hα 6563	−0.299	295.9 ± 5.3	286.5 ± 5.1	268.7 ± 7.7	268.7 ± 7.7	289.9 ± 6.3	278.8 ± 6.0
[N II] 6583	−0.301	10.4 ± 4.2	10.0 ± 4.0	11.8 ± 6.2	11.8 ± 6.2	2.6 ± 4.9	2.5 ± 4.7
[S II] 6716, 6731	−0.320	65.8 ± 6.2	63.3 ± 6.0	45 ± 10	45 ± 10	11.9 ± 1.6	11.4 ± 1.5
$F(\mathrm{H}\beta)$ (ergs s^{-1} cm^{-2})		(5.91 ± 0.23) × 10^{-16}		(3.22 ± 0.23) × 10^{-16}		(8.96 ± 0.31) × 10^{-16}	
$\mathrm{EW_e}(\mathrm{H}\beta)$ (Å)		83.9 ± 5.9		118 ± 19		105.6 ± 7.8	
$c(\mathrm{H}\beta)$		0.02		0		0	
$\mathrm{EW_{abs}}$ (Å)		2		0		4.7	

Notes: [a]Labelled as H II region No. 2 in Skillman et al. (1989). [b]Labelled as H II region No. 1 in Skillman et al. (1989). [c]Blended with [Ne III] λ3967.

evolution directly. The simplest 'closed-box' model (Schmidt 1963; Searle & Sargent 1972) can be written as $Z_\mathrm{O} = y_\mathrm{O} \ln(1/\mu)$, where Z_O is the oxygen mass fraction, y_O is the yield by mass and μ is the baryonic gas fraction equal to the ratio of the gas mass to the total mass in gas and stars.

In Figs 6(b)–(d), we have plotted the H I-gas-to-*B*-light ratio and parameters related to gas fraction against oxygen abundance. In the absence of measured optical colours for Cen A and Scl dIs to derive colour-based stellar mass-to-light ratios described by Bell & de Jong (2001), we compute stellar masses by simply assuming a constant stellar mass-to-*B*-light ratio equal to one. Our adopted value is within the range of stellar mass-to-*B*-light ratios derived by, for example, van Zee (2001) and Lee et al. (2003b). We compute total gas mass as $M_\mathrm{gas} = 1.36\,M_\mathrm{H\,I}$, which includes helium, but ignores molecular gas. Under the assumption of closed-box evolution, we have also plotted various curves with yields varying by a factor of 5. We find that nearby dIs (Lee et al. 2003b) and UGC dIs (van Zee, Haynes & Salzer 1997) span the range of yields shown. By inspection, $y_\mathrm{O} \approx (3 \pm 2) \times 10^{-3}$ is a good description of the data shown, in general agreement with the results of Lee et al. (2003b) and van Zee & Haynes (2006). The two Cen A dIs with direct abundances and low gas fractions are ESO 272−G025 and ESO 383−G087. Generally, Cen A dIs span the range of yields shown, whereas the small number of Scl dIs tend to cluster around the lower end of the yield range. However, these results are not definitive because of small-number statistics, and measurements of additional galaxies could strengthen possible differences in gas fractions between the two sets of dIs.

6.3 Relations with tidal index and projected distance

To explore further the effects of group environments on the properties of gas-rich dwarf galaxies, we examine various properties against tidal index and projected distance; the latter two parameters are defined and compiled in Karachentsev et al. (2004) and Karachentsev (2005). Briefly, the tidal index of a galaxy is the maximum value of an enhancement in mass density caused by all neighbouring galaxies. Objects with negative tidal indices are isolated in the field, and objects with positive tidal indices are found within group environments, and are likely undergoing a tidal interaction. Within each group, the projected distance of a galaxy, R_p, is given by $R_\mathrm{p} = D_\mathrm{m} \sin(\theta)$, where D_m is the distance of the main (or primary) group member to the Milky Way, and θ is the angular distance (in degrees) of the galaxy to the main member.

In Fig. 7, we have plotted various parameters against the tidal index and the projected distance of galaxies within each group. On the left side, we have plotted oxygen abundance, H I gas-to-light fraction, and the H I surface mass density as a function of tidal index in panels a, b and c, respectively. Values for the H I surface mass density were obtained from Karachentsev et al. (2004). We have compared Cen A and Scl group dwarfs against other dwarfs (as in Fig. 6), NGC 1705, and DDO 154. There are no obvious trends in the first two panels. We noted above that ESO 272−G025 and ESO 383−G087 appeared to have low gas fractions for their oxygen abundances, compared to other dwarfs. Both have negative tidal indices, which indicate only that there is no strong present-day tidal interactions. In panel c, the H I surface mass density appears to decrease with increasing positive tidal index, which is expected as strong tidal interactions remove gas from galaxies. We note that ESO 272−G025 (Cen A dI) has an unusually low H I surface mass density for its tidal index ($\Theta = -1.5$, $\log \sigma_\mathrm{H\,I} \approx 6$). This suggests that this dwarf may have encountered a strong interaction, which has reduced its H I content and has induced present-day star formation (i.e. presence of H II regions). Detailed spatially resolved observations would be very timely to confirm this scenario.

In Figs 7(d)–(g), we have plotted luminosity, H I-gas-to-light fraction, oxygen abundance, and the effective yield as a function of the projected distance, respectively. We have separated dwarfs in different groups by colour: Local Group (Milky Way + M31) in blue, M81 group dwarfs in brown, IC 342 + Maffei group dwarfs in dark green, and CVnI group dwarfs in black. Once more, there are no obvious trends; there is large scatter present in the plots of oxygen abundance and yield versus distance. Naturally, more data are required for examination and for improved statistics in an intergroup comparison. We note that ESO 381−G020 exhibits an unusually

Table 11. Line ratios and properties for H II regions in NGC 3109. RM92: Richer & McCall (1992). See Table 4 for additional comments, and Fig. 2 for slit orientations.

		(RM92 No. 8)[a]		(RM92 No. 5)[b]					
		A1		A3		B1		B2	
Property	$f(\lambda)$	F	I	F	I	F	I	F	I
[O II] 3727	+0.325	193.5 ± 2.9	184.0 ± 2.8	178.7 ± 3.3	168.7 ± 3.1	351 ± 28	289 ± 23	307 ± 53	258 ± 45
H 9 3835	+0.302	3.1 ± 1.3	8.1 ± 1.2	...	...	...	...	...	...
[Ne III] 3869	+0.294	23.3 ± 1.4	22.2 ± 1.3	30.1 ± 3.5	28.4 ± 3.3	...	...	...	...
H8 + He I 3889	+0.289	18.1 ± 1.4	23.3 ± 1.3	7.9 ± 2.8	19.0 ± 2.6	...	...	...	...
Hε + He I 3970[c]	+ 0.269	14.6 ± 1.3	19.7 ± 1.2	...	...	...	...	...	...
Hδ 4101	+0.232	19.9 ± 1.0	24.66 ± 0.95	9.6 ± 1.3	18.6 ± 1.2	...	...	...	...
Hγ 4340	+0.158	41.0 ± 1.4	44.1 ± 1.3	33.9 ± 1.6	40.0 ± 1.5	...	...	...	...
[O III] 4363	+0.151	<2.9	<2.8	<4.3	<4.1	...	...	...	...
He I 4471	+0.116	3.16 ± 0.58	3.01 ± 0.55	...	...	...	...	...	...
[He II] 4686	+0.050	13.9 ± 1.2	13.2 ± 1.1	...	...	...	...	...	...
Hβ 4861	0.000	100.0 ± 3.2	100.0 ± 3.0	100.0 ± 3.9	100.0 ± 3.7	100 ± 14	100 ± 12	100 ± 24	100 ± 18
[O III] 4959	−0.026	104.8 ± 6.8	99.7 ± 6.5	117.2 ± 6.8	110.6 ± 6.4	86 ± 13	71 ± 11	243 ± 25	183 ± 19
[O III] 5007	−0.038	308.4 ± 8.5	293.3 ± 8.1	350.4 ± 8.5	330.8 ± 8.0	247 ± 18	204 ± 15	649 ± 32	486 ± 24
He I 5876	−0.204	11.89 ± 0.87	11.31 ± 0.83	8.7 ± 1.4	8.2 ± 1.3	...	...	...	...
Hα 6563	−0.299	294.8 ± 6.8	283.5 ± 6.5	297.2 ± 5.4	283.2 ± 5.1	336 ± 15	287 ± 12	393 ± 30	285 ± 21
[N II] 6583	−0.301	13.2 ± 3.5	12.6 ± 3.3	2.2 ± 4.3	2.1 ± 4.1	...	...	...	...
He I 6678	−0.314	4.18 ± 0.94	3.98 ± 0.89	...	...	...	...	...	...
[S II] 6716	−0.319	20.3 ± 1.7	19.3 ± 1.6	12.7 ± 1.5[d]	12.0 ± 1.4	...	...	...	...
[S II] 6731	−0.321	12.6 ± 1.5	12.0 ± 1.4	12.7 ± 1.5[d]	12.0 ± 1.4	...	...	...	...
[Ar III] 7136	−0.375	8.6 ± 1.1	8.2 ± 1.1	9.6 ± 1.8	9.1 ± 1.7	...	...	...	...
F(Hβ) (ergs s^{-1} cm^{-2})		(2.239 ± 0.073) × 10^{-15}		(1.073 ± 0.042) × 10^{-15}		(1.09 ± 0.16) × 10^{-16}		(6.1 ± 1.5) × 10^{-17}	
EW$_e$(Hβ) (Å)		38.8 ± 1.6		33.7 ± 1.6		9.4 ± 1.4		6.3 ± 1.5	
c(Hβ)		0		0		0		0.14	
EW$_{abs}$ (Å)		2		2		2		2	

		(RM92 No. 6)[e]				(RM92 No. 1)[f]	
		B4		B5		B6	
Property	$f(\lambda)$	F	I	F	I	F	I
[O II] 3727	+0.325	201.9 ± 4.4	192.2 ± 4.2	274.5 ± 3.6	275.6 ± 3.6	265.2 ± 3.4	268.9 ± 3.5
H 9 3835	+0.302	...	...	...	...	2.4 ± 1.1	5.0 ± 1.1
[Ne III] 3869	+0.294	19.8 ± 2.1	18.9 ± 2.0	12.1 ± 1.6	12.1 ± 1.6	18.1 ± 1.3	18.3 ± 1.3
H8 + He I 3889	+0.289	20.6 ± 2.1	22.5 ± 2.0	11.6 ± 1.6	18.4 ± 1.6	14.7 ± 1.2	18.0 ± 1.2
Hε + He I 3970[c]	+ 0.269	19.0 ± 2.5	21.4 ± 2.4	8.8 ± 1.3	15.3 ± 1.3	14.5 ± 1.2	17.6 ± 1.2
Hδ 4101	+0.232	23.7 ± 2.6	26.3 ± 2.5	18.7 ± 1.7	24.5 ± 1.7	22.1 ± 1.2	24.7 ± 1.2
Hγ 4340	+0.158	50.1 ± 2.3	51.4 ± 2.2	41.0 ± 1.8	45.2 ± 1.8	40.2 ± 1.4	42.4 ± 1.4
[O III] 4363	+0.151	<7.1	<6.8	<3.9	<3.8	<3.4	<3.4
Hβ 4861	0.000	100.0 ± 3.9	100.0 ± 3.7	100.0 ± 3.7	100.0 ± 3.5	100.0 ± 3.1	100.0 ± 3.1
[O III] 4959	−0.026	111.7 ± 7.2	106.3 ± 6.9	58.3 ± 3.6	55.4 ± 3.4	107.9 ± 6.0	105.9 ± 5.9
[O III] 5007	−0.038	327.4 ± 9.1	311.6 ± 8.7	172.9 ± 4.6	163.9 ± 4.4	319.6 ± 7.5	313.4 ± 7.4
He I 5876	−0.204	10.3 ± 2.5	9.8 ± 2.4	8.0 ± 1.2	7.4 ± 1.1	10.20 ± 0.90	9.85 ± 0.87
Hα 6563	−0.299	296.9 ± 6.3	286.6 ± 6.0	312.2 ± 6.4	286.1 ± 5.8	297.3 ± 4.9	285.1 ± 4.7
[N II] 6583	−0.301	5.5 ± 5.1	5.2 ± 4.9	8.8 ± 5.1	8.0 ± 4.6	6.7 ± 3.9	6.4 ± 3.7
[S II] 6716	−0.319	18.2 ± 2.0[d]	17.3 ± 1.9	38.7 ± 3.3[d]	35.0 ± 3.0	16.7 ± 1.7	16.0 ± 1.6
[S II] 6731	−0.321	18.2 ± 2.0[d]	17.3 ± 1.9	38.7 ± 3.3[d]	35.0 ± 3.0	10.0 ± 1.5	9.6 ± 1.4
[Ar III] 7136	−0.375	...	...	6.2 ± 1.1	5.57 ± 0.99	6.9 ± 1.2	6.6 ± 1.1
[O II] 7320, 7330	−0.400	...	...	...	...	6.8 ± 1.4	6.5 ± 1.3
F(Hβ) (ergs s^{-1} cm^{-2})		(9.14 ± 0.35) × 10^{-16}		(2.005 ± 0.074) × 10^{-15}		(2.369 ± 0.073) × 10^{-15}	
EW$_e$(Hβ) (Å)		41.5 ± 2.0		41.1 ± 1.9		122.5 ± 9.1	
c(Hβ)		0		0.07		0.04	
EW$_{abs}$ (Å)		2.1		2		2	

Notes: [a]Labelled as complex D2H5 in Bresolin et al. (1993), and H II #26 in Peña et al. (2006). [b]Labelled as complex F1H3 in Bresolin et al. (1993), and H II #13 in Peña et al. (2006). [c]Blended with [Ne III] λ3967. [d][S II] unresolved. [e]Labelled as complex D2H5 in Bresolin et al. (1993), and H II #18 in Peña et al. (2006). [f]Labelled as complex F1H4 in Bresolin et al. (1993), and H II #8 in Peña et al. (2006).

high effective yield for its projected distance (≈0.9 Mpc), although the dI does not appear to have any other unusual properties.

Although a number of Cen A dwarfs in our sample have positive tidal indices, there is little to separate these galaxies from those with negative tidal indices in the luminosity–metallicity, metallicity–gas fraction and metallicity–tidal index diagrams. There is also no clear trend between the current chemical enrichment (as represented by either oxygen abundance or yield) with the projected distance of

Table 12. Line ratios and properties for H II regions in Sextans B. SHK91: Strobel et al. (1991). See Table 4 for additional comments, and Fig. 2 for slit orientations.

		Long-slit orientation A[a]					
		SHK91 No. 1[b]		SHK91 No. 2[c]		SHK91 No. 5[d]	
Property	$f(\lambda)$	F	I	F	I	F	I
[O II] 3727	+0.325	291.5 ± 5.3	282.4 ± 5.1	310 ± 11	322 ± 11	263.8 ± 5.2	255.5 ± 5.0
[Ne III] 3869	+0.294	15.0 ± 2.2	14.5 ± 2.1	...	...	18.3 ± 2.7	17.7 ± 2.6
H8 + He I 3889	+0.289	12.8 ± 2.1	19.1 ± 2.0	...	...	23.1 ± 2.8	27.0 ± 2.7
Hε + He I 3970[e]	+0.269	8.3 ± 2.2	14.7 ± 2.1	...	...	13.7 ± 2.5	18.0 ± 2.4
Hδ 4101	+0.232	14.2 ± 1.7	19.8 ± 1.6	...	...	22.0 ± 1.9	25.8 ± 1.8
Hγ 4340	+0.158	36.2 ± 1.7	39.9 ± 1.6	27.0 ± 4.8	37.9 ± 4.7	42.8 ± 2.0	45.3 ± 1.9
[O III] 4363	+0.151	<4.7	<4.5	...	...	<6.1	<5.9
Hβ 4861	0.000	100.0 ± 3.3	100.0 ± 3.2	100.0 ± 5.5	100.0 ± 5.0	100.0 ± 3.5	100.0 ± 3.4
[O III] 4959	−0.026	60.3 ± 3.5	57.9 ± 3.4	48.0 ± 4.6	43.5 ± 4.2	82.2 ± 5.2	79.6 ± 5.0
[O III] 5007	−0.038	171.9 ± 4.5	165.1 ± 4.3	153.3 ± 5.6	138.1 ± 5.0	241.4 ± 6.6	233.8 ± 6.4
Hα 6563	−0.299	296.0 ± 6.4	284.6 ± 6.1	347 ± 12	286.3 ± 9.8	292.7 ± 5.4	285.4 ± 5.2
[N II] 6583	−0.301	2.2 ± 5.0	2.1 ± 4.8	26.1 ± 9.3	21.2 ± 7.6	3.9 ± 4.3	3.8 ± 4.2
[S II] 6716, 6731	−0.320	25.1 ± 3.9	24.0 ± 3.7	...	...	28.6 ± 4.0	27.7 ± 3.9
$F(H\beta)$ (ergs s^{-1} cm^{-2})		(1.722 ± 0.056) × 10^{-15}		(4.15 ± 0.23) × 10^{-16}		(1.482 ± 0.052) × 10^{-15}	
$EW_e(H\beta)$ (Å)		49.9 ± 2.2		21.4 ± 1.3		61.9 ± 3.3	
$c(H\beta)$		0.01		0.17		0	
EW_{abs} (Å)		2		2		2	

		Long-slit orientation B					
		SHK91 No. 5 narrow[f]		SHK91 No. 5 wide[g]		SHK91 No. 10[h]	
Property	$f(\lambda)$	F	I	F	I	F	I
[O II] 3727	+0.325	237.1 ± 5.7	237.1 ± 5.7	260.4 ± 4.4	260.4 ± 4.4	370.6 ± 6.7	370.6 ± 6.7
H 9 3835	+0.302	7.5 ± 2.5	7.5 ± 2.5	4.2 ± 1.8	4.2 ± 1.8	5.9 ± 1.6	5.9 ± 1.6
[Ne III] 3869	+0.294	19.3 ± 2.8	19.3 ± 2.8	21.5 ± 2.0	21.5 ± 2.0	4.6 ± 1.6	4.6 ± 1.6
H8 + He I 3889	+0.289	19.4 ± 2.8	19.4 ± 2.8	18.5 ± 2.0	18.5 ± 2.0	14.1 ± 1.9	14.1 ± 1.9
Hε + He I 3970[e]	+0.269	17.9 ± 2.7	17.9 ± 2.7	16.4 ± 1.9	16.4 ± 1.9	9.8 ± 1.4	9.8 ± 1.4
Hδ 4101	+0.232	21.9 ± 2.9	21.9 ± 2.9	25.9 ± 2.2	25.9 ± 2.2	21.0 ± 1.7	21.0 ± 1.7
Hγ 4340	+0.158	43.1 ± 2.5	43.1 ± 2.5	43.8 ± 1.7	43.8 ± 1.7	43.2 ± 1.5	43.2 ± 1.5
[O III] 4363	+ 0.151	< 7.1	< 7.1	4.2 ± 1.4	4.2 ± 1.4	< 3.1	< 3.1
Hβ 4861	0.000	100.0 ± 3.3	100.0 ± 3.3	100.0 ± 3.3	100.0 ± 3.3	100.0 ± 3.6	100.0 ± 3.6
[O III] 4959	−0.026	86.0 ± 5.2	86.0 ± 5.2	82.4 ± 4.7	82.4 ± 4.7	23.3 ± 2.0	23.3 ± 2.0
[O III] 5007	−0.038	264.3 ± 6.7	264.3 ± 6.7	237.7 ± 5.9	237.7 ± 5.9	72.5 ± 2.5	72.5 ± 2.5
He I 5876	−0.204	...	...	8.0 ± 1.5	8.0 ± 1.5	...	...
Hα 6563	−0.299	265.3 ± 5.5	265.3 ± 5.5	265.1 ± 4.8	265.1 ± 4.8	283.6 ± 5.7	283.6 ± 5.7
[N II] 6583	−0.301	1.0 ± 4.4	1.0 ± 4.4	5.9 ± 3.8	5.9 ± 3.8	8.8 ± 4.5	8.8 ± 4.5
[S II] 6716, 6731	−0.320	21.2 ± 3.4	21.2 ± 3.4	31.3 ± 3.2	31.3 ± 3.2	35.3 ± 2.8	35.3 ± 2.8
$F(H\beta)$ (ergs s^{-1} cm^{-2})		(3.24 ± 0.11) × 10^{-16}		(1.043 ± 0.035) × 10^{-15}		(1.294 ± 0.047) × 10^{-15}	
$EW_e(H\beta)$ (Å)		96.4 ± 6.6		96.0 ± 6.4		57.2 ± 3.0	
$c(H\beta)$		0		0		0	
EW_{abs} (Å)		0		0		0	

Notes: [a]The long-slit also went through H II region SHK91 No. 4, but only weak [O II] λ3727 and Hα emission lines were detected. [b]Labelled as H II region No. 1 in Skillman et al. (1989). [c]Labelled as H II region No. 4 in Skillman et al. (1989). [d]Labelled as H II region No. 2 in Skillman et al. (1989), and the 'primary' H II region in Stasińska et al. (1986) and Moles et al. (1990). [e]Blended with [Ne III] λ3967. [f]'Narrow' extraction aperture: 10 pixels (1.6 arcsec). [g]'Wide' extraction aperture: 44 pixels (7.0 arcsec). [h]Labelled as H II region No. 3 in Skillman et al. (1989).

galaxies within each group. Because of low-number statistics, it is difficult to say at the present time whether any separation of Cen A dwarfs and Scl dwarfs in these diagnostics is meaningful.

7 CONCLUSIONS

Results of optical spectroscopy of H II regions from eight dwarf galaxies in the Cen A group are presented. For ESO 272−G025 and ESO 324−G024, direct oxygen abundances of $12 + \log(O/H) = 7.76 \pm 0.09$ and 7.94 ± 0.11 are derived, respectively. Bright-line abundances for the remaining galaxies are derived with the McGaugh and the Pilyugin calibrations. We have also considered data for additional Cen A dIs and Sculptor group dIs from the literature. For their galaxy luminosities, we have found that direct or [O III] λ4363 oxygen abundances agree well with the luminosity–metallicity relationship for dwarf irregular galaxies. Despite large tidal indices for a number of Cen A dwarf galaxies, there is no difference between galaxies with positive tidal indices galaxies with negative tidal indices in the luminosity–metallicity, metallicity–gas fraction and metallicity–tidal index diagrams. As expected in strong tidal interactions, the H I surface mass density appears to decrease with increasing positive tidal index. We have also examined global properties of dwarf galaxies based on their intra-group properties. There are no obvious trends in plots of luminosity,

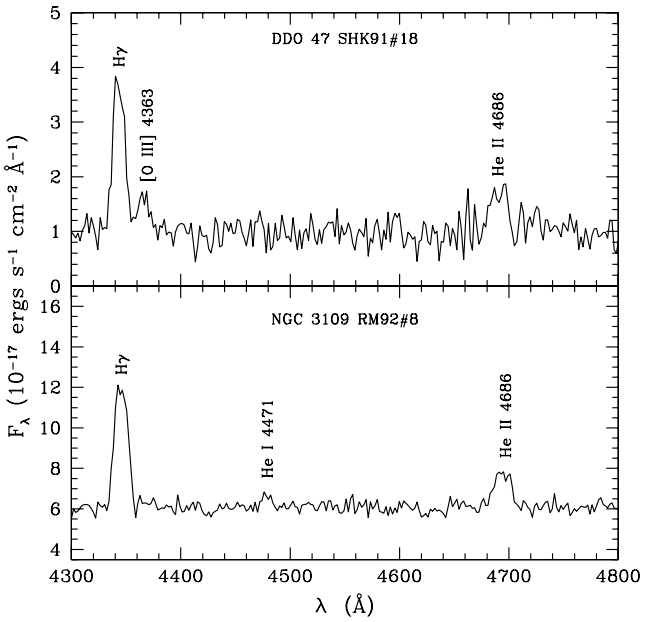

Figure 5. Spectra of H II regions — DDO 47 SHK91 No. 18, and NGC 3109 RM92 No. 8 — between 4300 and 4800 Å. The emission lines Hγ, [O III] λ4363, He I λ4471 and He II λ4686 are labelled.

H I-to-*B*-light ratio, oxygen abundance, and yield against projected distance of galaxies within nearby groups. We also report spectra and abundances for three nearby dwarf irregular galaxies: DDO 47, NGC 3109 and Sextans B. Our direct oxygen abundance (7.92 $\pm$ 0.06) for DDO 47 agrees with the measurement previously reported by Skillman et al. (1989). For Sextans B, our direct oxygen abundance (7.80 $\pm$ 0.13) is consistent with the low value reported by Skillman et al. (1989), and agrees with abundances reported by Kniazev et al. (2005) and Magrini et al. (2005).

ACKNOWLEDGMENTS

We thank the anonymous referee for comments which improved the presentation of the manuscript. HL is supported by the Gemini Observatory, which is operated by the Association of Universities for Research in Astronomy, Inc., on behalf of the international Gemini partnership of Argentina, Australia, Brazil, Canada, Chile, the United Kingdom and the United States of America. We are grateful to ESO for awarded telescope time, and we thank Lisa Germany, George Hau and the staff at ESO La Silla for help with the observations. Partial support for this work was provided by NASA through grant GO-08192.97A from the Space Telescope Science Institute, which is operated by the Association of Universities for Research in Astronomy, Inc., under NASA contract NAS5-26555. DBZ acknowledges support from the National Science Foundation Postdoctoral Fellowship. EKG appreciates support by the Swiss National Science Foundation through grants 200021-101924 and 200020-105260. HL is grateful for support from the Max-Planck-Institute for Astronomy where this project was begun, for partial support from a NASA LTSARP grant NAG 5-9221, and from the University of Minnesota. HL also thanks Stephanie Côté and Evan Skillman for providing their Hα images, and Liese van Zee for discussions regarding bright-line calibrations. Some data were accessed as Guest User, Canadian Astronomy Data Center, which is operated by the Dominion Astrophysical Observatory for the National Research Council of Canada's Herzberg Institute of Astrophysics. This research has made use of the NASA/IPAC Extragalactic Database,

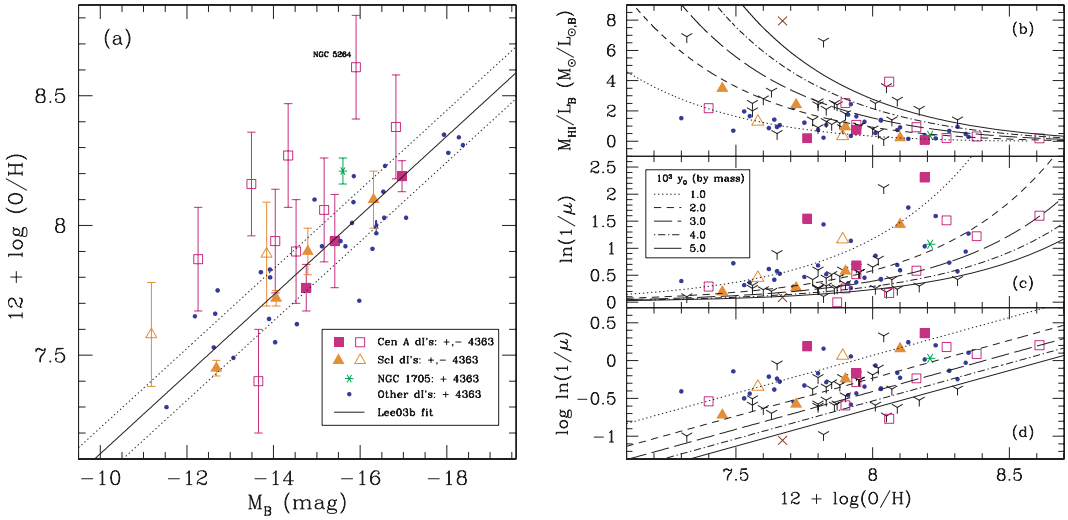

Figure 6. Panel (a): *B*-band luminosity–metallicity relation for dwarf irregular galaxies. Squares mark locations of Cen A dwarf galaxies from the present data and Lee et al. (2003a). Triangles mark locations of Sculptor group (Scl) dwarf galaxies from Skillman et al. (2003b) and Lee et al. (2003a). Small circles indicate nearby dwarf irregular galaxies in the Local Volume (Lee et al. 2003a,b) with updates to WLM and NGC 6822 (Lee et al. 2005, 2006a); DDO 47 and Sextans B from the present spectra have also been included. Additional objects have been added to the sample of 'nearby dwarfs'; see text for discussion. [O III] λ4363 detections are shown as filled symbols. The star marks the location of the nearby dwarf starburst galaxy NGC 1705 (Lee & Skillman 2004). The solid line is a fit to a sample of nearby dwarf irregulars described in Lee et al. (2003b). We note that Cen A and Scl group dwarfs with [O III] λ4363 abundances are within 0.1 dex (dotted lines) of the fit. NGC 5264 exhibits an unusually high oxygen abundance for its luminosity, although the spectra are of low signal-to-noise. Panels (b–d): gas-to-*B* light fraction and gas fraction parameters as a function of oxygen abundance. Symbols are the same as in panel (a); additional Y symbols mark locations of dwarf irregulars from van Zee et al. (1997) and van Zee & Haynes (2006), and a cross marks the location of the gas-rich dwarf irregular galaxy DDO 154 (van Zee et al. 1997; Kennicutt & Skillman 2001). Error bars have not been plotted to aid visibility. Curves of different line type mark loci of closed-box chemical evolution models with different values of effective oxygen yields (by mass) as indicated (see also Lee et al. 2003b).

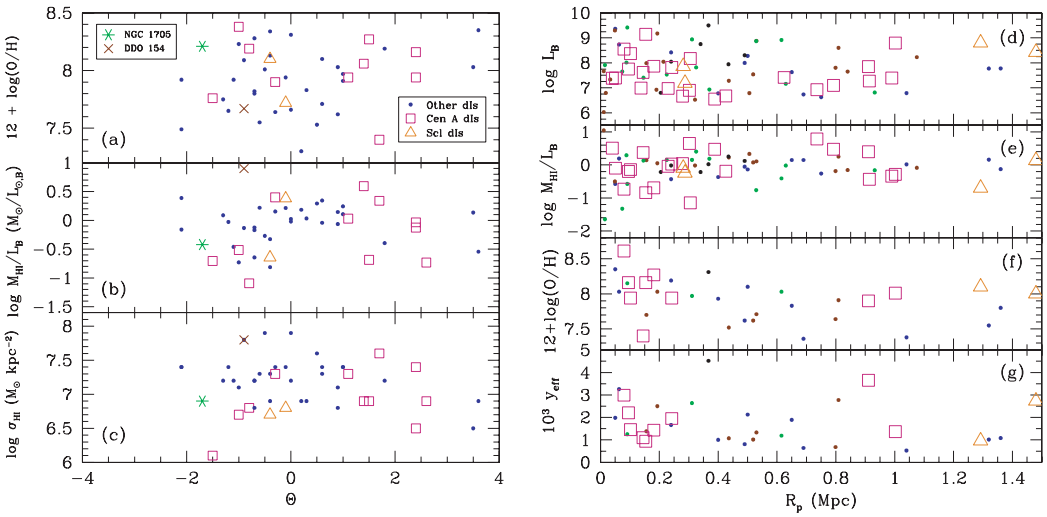

Figure 7. Left-hand panels: oxygen abundance (a), H I gas-to-*B* light fraction (b), and H I surface mass density (c) against tidal index. Symbols are the same as in Fig. 6. Right-hand panels: optical *B* luminosity in solar units (d), H I gas-to-*B* light fraction in solar units (e), oxygen abundance (f) and effective chemical yield (g) as a function of projected distance of dwarf galaxies to the primary member in their respective group. Data are culled from the assigned membership of galaxies into groups described by Karachentsev (2005). Cen A group and Scl group dwarfs are marked as open squares in magenta and open triangles in orange, respectively. Filled circles denote: Local Group (Milky Way + M31) dwarfs in blue, M81 group dwarfs in brown, IC 342 + Maffei group dwarfs in dark green and CVnI group dwarfs in black.

Table 13. Ionic and total nebular abundances for Cen A dwarf irregular galaxies. Direct ([O III] λ4363) oxygen abundances are shown with two uncertainties. The first uncertainty is the formal uncertainty in the derivation. In parentheses is the range of possible values, expressed by the maximum and minimum values of the oxygen abundance. For the McGaugh bright-line calibration, two abundances are shown to reflect the lower and upper branches, respectively. The underlined value reflects the choice as judged from the I([N II] λ6583)/I([O II] λ3727) ratio (e.g. McCall et al. 1985; McGaugh 1994; van Zee et al. 1998; Lee et al. 2003b). In the absence of [N II] λ6583, no choice is assigned, and abundances from both branches are given.

Property	AM 1318−444 No. 1	ESO 272−G025 No. 1	ESO 272−G025 No. 2	ESO 274−G001 No. 1	ESO 274−G001 No. 4[a]	ESO 274−G001 No. 5
$T_e(O^{+2})$ (K)	<15050	15700 ± 210	...	...	<18700	...
$T_e(O^{+})$ (K)	<13540	13990 ± 190	...	...	<16100	...
O^+/H (× 10^5)	>2.8	2.19 ± 0.92	...	...	>2.58	...
O^{+2}/H (× 10^5)	>2.0	3.6 ± 1.0	...	...	>1.57	...
O/H (× 10^5)	>4.8	5.7 ± 1.4	...	...	>4.15	...
12 + log(O/H)	>7.68	$7.76 \pm 0.09(^{+0.11}_{-0.15})$	...	...	>7.62	...
12 + log(O/H) M91[b]	7.87/8.70	8.01/8.57	8.14/8.56	7.96/8.79	8.16/8.51	7.90/8.63
12 + log(O/H) P00,P01a[c]	7.86	7.84	...	...	8.15/8.24	7.72/8.50

Property	ESO 274−G001 No. 6	ESO 274−G001 No. 7	ESO 274−G001 No. 8	ESO 324−G024 No. 1	ESO 324−G024 No. 2	ESO 324−G024 No. 3
$T_e(O^{+2})$ (K)	...	...	...	...	...	...
$T_e(O^{+})$ (K)	...	...	...	...	...	...
O^+/H (× 10^5)	...	...	...	...	...	...
O^{+2}/H (× 10^5)	...	...	...	...	...	...
O/H (× 10^5)	...	...	...	...	...	...
12 + log(O/H)	...	...	...	...	...	...
12 + log(O/H) M91[b]	8.39/8.39	8.27/8.49	7.92/8.81	8.17/8.54	8.06/8.66	8.06/8.65
12 + log(O/H) P00[c]	...	...	...	...	...	...

Property	ESO 324−G024 No. 4	ESO 324−G024 No. 5	ESO 325−G011 No. 1	ESO 325−G011 No. 2 No. 3	ESO 325−G011 No. 4	ESO 325−G011
$T_e(O^{+2})$ (K)	13400 ± 1400	12500 ± 1800	...	...	...	<21100
$T_e(O^{+})$ (K)	12400 ± 1300	11700 ± 1700	...	...	...	<17800
O^+/H (× 10^5)	2.45 ± 0.92	3.4 ± 1.8	...	...	...	>1.13
O^{+2}/H (× 10^5)	5.2 ± 1.4	6.3 ± 2.4	...	...	...	>1.16
O/H (× 10^5)	7.6 ± 1.7	9.7 ± 3.0	...	...	...	>2.29
12 + log(O/H)	$7.88 \pm 0.09(^{+0.10}_{-0.14})$	$7.99 \pm 0.11(^{+0.14}_{-0.20})$	...	...	...	>7.36
12 + log(O/H) M91[b]	7.89/8.64	7.93/8.62	8.05/8.72	7.92/8.65	7.95/8.70	7.86/8.68
12 + log(O/H) P00[c]	7.72	7.77	...	7.85	8.15	7.80

Table 13 – *continued*

Property	ESO 325−G011 No. 5[d]	ESO 381−G020 No. 1	ESO 381−G020 No. 2	ESO 381−G020 No. 3	ESO 381−G020 No. 4	ESO 381−G020 No. 5
$T_e(O^{+2})$ (K)	...	<24700	...	<19000	...	...
$T_e(O^{+})$ (K)	...	<20300	...	<16300	...	...
O^{+}/H ($\times 10^5$)	...	>0.69	...	> 1.34	...	...
O^{+2}/H ($\times 10^5$)	...	>1.29	...	> 1.61	...	...
O/H ($\times 10^5$)	...	>1.98	...	>2.95	...	...
12 + log(O/H)	...	>7.30	...	>7.47	...	...
12 + log(O/H) M91[b]	7.96/8.78	7.96/8.61	8.32/8.39	7.87/8.67	8.16/8.63	7.43/8.86
12 + log(O/H) P00[c]	...	7.79	...	7.77	...	7.31

Property	ESO 381−G020 No. 6	IC 4247 No. 1	IC 4247 No. 2	IC 4316 No. 1	IC 4316 No. 2	IC 4316 No. 3
$T_e(O^{+})$ (K)	...	...	...	...	<10800	...
$T_e(O^{+})$ (K)	...	...	...	...	<10800	...
O^{+}/H ($\times 10^5$)	...	...	...	...	> 8.11	...
O^{+2}/H ($\times 10^5$)	...	...	...	...	> 6.04	...
12 + log(O/H)	...	...	...	...	>8.15	...
12 + log(O/H) M91[b]	7.46/8.89	8.24/8.44	8.29/8.50	8.33/8.49	8.05/8.58	8.34/8.38
12 + log(O/H) P00[c]	7.38	...	...	...	8.01	...

Property	IC 4316 No. 4	IC 4316 No. 5	IC 4316 No. 6
$T_e(O^{+2})$ (K)	...	...	...
$T_e(O^{+})$ (K)	...	...	...
O^{+}/H ($\times 10^5$)	...	...	...
O^{+2}/H ($\times 10^5$)	...	...	...
12 + log(O/H)	...	...	...
12 + log(O/H) M91[b]	8.07/8.62	8.11/8.58	8.07/8.60
12 + log(O/H) P00[c]	...	...	8.22

Notes: [a]May be a candidate for a supernova remnant; see text in Section 5. [b]McGaugh (1991) bright-line calibration; see also Kobulnicky et al. (1999). [c]Bright-line calibration: lower branch – Pilyugin (2000); upper branch – Pilyugin (2001). [d]Background galaxy with $v_\odot \approx 26\,200\,\mathrm{km\,s^{-1}}$.

Table 14. Ionic and total abundances for observed H II regions in DDO 47, NGC 3109 and Sextans B. See Table 13 for general comments. DDO 47 – SHK91 refers to the identifications in Strobel et al. (1991); see also Figs 2 and 10. NGC 3109 – Figs 2 and 11. Sextans B – SHK refers to the identifications in Strobel et al. (1991); see also Figs 2 and 12.

Property	DDO 47 SHK91 No. 16	DDO 47 SHK91 No. 17	DDO 47 SHK91 No. 18	NGC 3109 (RM92 No. 8) A1	NGC 3109 (RM92 No. 5) A3	NGC 3109 B1
$T_e(O^{+2})$ (K)	...	...	13910 ± 940	<11300	<12400	...
$T_e(O^{+})$ (K)	...	...	12740 ± 860	<10900	<11700	...
O^{+}/H ($\times 10^5$)	...	...	0.94 ± 0.22	>4.8	>3.3	...
O^{+2}/H ($\times 10^5$)	...	...	7.4 ± 1.2	>6.9	>5.8	...
O/H ($\times 10^5$)	...	...	8.3 ± 1.3	>11.7	>9.1	...
12 + log(O/H)	...	...	$7.92 \pm 0.06(^{+0.07}_{-0.08})$	>8.07	>7.96	...
12 + log(O/H) M91[a]	7.86/8.72	8.11/8.51	7.93/8.60	7.87/8.66	7.88/8.65	7.98/8.64
12 + log(O/H) P00[b]	7.88	7.93	7.74	7.74	7.73	7.98

Table 14 – *continued*

Property	NGC 3109 B2	NGC 3109 (RM92 No. 6) B4	NGC 3109 (RM92 No. 6) B5	NGC 3109 (RM92 No. 1) B6	Sextans B SHK91 No. 1	Sextans B SHK91 No. 2
$T_e(O^{+2})$ (K)	...	<15800	<16400	<11900	<17800	...
$T_e(O^{+})$ (K)	...	<14100	<14500	<11300	<15400	...
O^+/H ($\times 10^5$)	...	>2.0	>2.6	>6.0	>2.2	...
O^{+2}/H ($\times 10^5$)	...	>2.9	>1.4	>6.3	>1.2	...
O/H ($\times 10^5$)	...	>4.9	> 4.0	>12.3	>3.4	...
12 + log(O/H)	...	>7.69	>7.60	>8.09	>7.53	...
12 + log(O/H) M91[a]	8.24/8.42	7.91/8.63	7.92/8.69	8.06/8.56	7.93/8.68	7.98/8.67
12 + log(O/H) P00,P01a[b]	8.00/8.25	7.77	7.97	7.94	7.99	8.14

Property	Sextans B SHK91 No. 5[c]	Sextans B SHK91 No. 5[d,e]	Sextans B SHK91 No. 5[d,f]	Sextans B SHK91 No. 10
$T_e(O^{+2})$ (K)	<17100	<17700	14380 ± 240	<23700
$T_e(O^{+})$ (K)	<15000	<15400	13060 ± 210	<19600
O^+/H ($\times 10^5$)	>2.2	>1.9	3.5 ± 1.9	>1.5
O^{+2}/H ($\times 10^5$)	>1.8	>1.9	2.8 ± 1.1	>0.28
O/H ($\times 10^5$)	>4.0	>3.7	6.3 ± 2.2	>1.76
12 + log(O/H)	> 7.60	>7.57	$7.80 \pm 0.13(^{+0.14}_{-0.21})$	>7.25
12 + log(O/H) M91[c]	7.95/8.64	7.94/8.64	7.96/8.63	8.05/8.68
12 + log(O/H) P00[d]	7.90	7.86	7.91	...

Notes:[a]McGaugh (1991) bright-line calibration.[b]Bright-line calibration: lower branch – Pilyugin (2000); upper branch – Pilyugin (2001).[c]Slit orientation A.[d]Slit orientation B.[e]'Narrow' extraction aperture of total 10 pixels.[f]'Wide' extraction aperture of total 44 pixels.

which is operated by the Jet Propulsion Laboratory, California Institute of Technology, under contract with the National Aeronautics and Space Administration.

REFERENCES

Aller L. H., 1984, Physics of Thermal Gaseous Nebulae. Reidel, Dordrecht
Asplund M., Grevesse N., Sauval A. J., Allende Prieto C., Kiselman D., 2004, A&A, 417, 751
Banks G. D. et al., 1999, ApJ, 524, 612
Barnes D. G., de Blok W. J. G., 2001, AJ, 122, 825
Bell E. F., de Jong R. S., 2001, ApJ, 550, 212
Bothun G. D., Mould J. R., Caldwell N., MacGillivray H. T., 1986, AJ, 92, 1007
Bouchard A., Jerjen H., Da Costa G. S., Ott J., 2007, AJ, 133, 261
Bresolin F., Capaccioli M., Piotto G., 1993, AJ, 105, 1779
Campbell A., Terlevich R. J., Melnick J., 1986, MNRAS, 223, 811
Cardelli J. A., Clayton G. C., Mathis J. S., 1989, ApJ, 345, 245
Carignan C., 1985, ApJ, 299, 59
Côté S., Freeman K. C., Carignan C., Quinn P. J., 1997, AJ, 114, 1313
Côté S., Carignan C., Freeman K. C., 2000, AJ, 120, 3027
de Vaucouleurs G., 1979, AJ, 84, 1270
de Vaucouleurs G., de Vaucouleurs A., Corwin H., Jr, Buta R. J., Paturel G., Fouqué P., 1991, Third Reference Catalogue of Bright Galaxies. Springer, New York
Dinerstein H. L., 1990, in Thronson H. A., Shull J. M., eds, The Interstellar Medium in Galaxies. Kluwer, Dordrecht, p. 257
Dopita M. A., Binette L., D'Odorico S., Benvenuti P., 1984, ApJ, 276, 653
Garnett D. R., 1992, AJ, 103, 1330
Graham J. A., 1979, ApJ, 232, 60
Grebel E. K., 1997, Rev. Mod. Astron., 10, 29
Grebel E. K., 1999, in Whitelock P., Cannon R., eds, IAU Symp. 192, The Stellar Content of the Local Group. Astron. Soc. Pac., San Francisco, p. 17
Grebel E. K., 2001a, Ap&SS, 277, 231
Grebel E. K., 2001b, in De Boer K. S., Dettmar R.-J., Klein U., eds, Dwarf Galaxies and the Environment. Shaker Verlag, Aachen, p. 45
Grebel E. K., Seitzer P., Dolphin A., Geisler D., Guhathakurta P., Hodge P., Karachentseva I., Sarajedini A., 2000, in Alloin D., Olsen K., Galaz G., eds, ASP Conf. Ser. Vol. 221, Stars, Gas and Dust in Galaxies: Exploring the Links. Astron. Soc. Pac., San Francisco, p. 147
Grebel E. K., Gallagher J. S., Harbeck D. R., 2003, AJ, 125, 1926
Grossi M., Disney M. J., Pritzl B. J., Knezek P. M., Gallagher J. S., Minchin R. F., Freeman K. C., 2007, MNRAS, 374, 107
Hoffman G. L., Salpeter E. E., Farhat B., Roos T., Williams H., Helou G., 1996, ApJS, 105, 269
Jenkins C. R., 1987, MNRAS, 226, 341
Jerjen H., Binggeli B., Freeman K. C., 2000, AJ, 119, 593
Jobin M., Carignan C., 1990, AJ, 100, 648
Karachentsev I. D., 2005, AJ, 129, 178
Karachentsev I. D. et al., 2002a, A&A, 383, 125
Karachentsev I. D. et al., 2002b, A&A, 385, 21
Karachentsev I. D. et al., 2002c, A&A, 389, 812
Karachentsev I. D. et al., 2003a, A&A, 398, 467
Karachentsev I. D. et al., 2003b, A&A, 398, 479
Karachentsev I. D., Karachentseva V. E., Huchtmeier W. K., Makarov D. I., 2004, AJ, 127, 2031
Karachentsev I. D. et al., 2007, ApJ, 133, 504
Kennicutt R. C., Skillman E. D., 1993, ApJ, 411, 655
Kennicutt R. C., Skillman E. D., 2001, AJ, 121, 1461
Kniazev A. Y., Pustilnik S. A., Grebel E. K., Lee H., Pramskij A. G., 2004, ApJS, 153, 429
Kniazev A. Y., Grebel E. K., Pustilnik S. A., Pramskij A. G., Zucker D. B., 2005, AJ, 130, 1558
Kobulnicky H. A., Kennicutt R. C., Jr, Pizagno J. L., 1999, ApJ, 514, 544
Lee H., Skillman E. D., 2004, ApJ, 614, 698
Lee H., Grebel E. K., Hodge P. W., 2003a, A&A, 401, 141
Lee H., McCall M. L., Kingsburgh R., Ross R., Stevenson C. C., 2003b, AJ, 125, 146
Lee H., McCall M. L., Richer M. G., 2003c, AJ, 125, 2975

Lee H., Skillman E. D., Venn K. A., 2005, ApJ, 620, 223
Lee H., Skillman E. D., Venn K. A., 2006a, ApJ, 642, 813
Lee H., Skillman E. D., Cannon J. M., Jackson D. C., Gehrz R. D., Polomski E. F., Woodward C. E., 2006b, ApJ, 647, 970
McCall M. L., Rybski P. M., Shields G. A., 1985, ApJS, 57, 1
McGaugh S. S., 1991, ApJ, 380, 140
McGaugh S. S., 1994, ApJ, 426, 135
Magrini L., Leisy P., Corradi R. L. M., Perinotto M., Mampaso A., Vílchez J. M., 2005, A&A, 443, 115
Martin C., 1997, ApJ, 491, 561
Meier D. L. et al., 1989, AJ, 98, 27
Meléndez J., 2004, ApJ, 615, 1042
Mirabel I. F. et al., 1999, A&A, 341, 667
Moles M., Aparicio A., Masegosa J., 1990, A&A, 228, 310
Mulchaey J. S., 2000, ARA&A, 38, 289
Olive K. A., Skillman E. D., 2001, New Astron., 6, 119
Osterbrock D. E., 1989, Astrophysics of Gaseous Nebulae and Active Galactic Nuclei. University Science Books, Mill Valley
Pagel B. E. J., Edmunds M. G., Blackwell D. E., Chun M. S., Smith G., 1979, MNRAS, 189, 95
Peña M., Richer M. G., Stasińska G., 2006, A&A, in press (astro-ph/0612553)
Peng E. W., Ford H. W., Freeman K. C., White R. L., 2002, AJ, 124, 3144
Pilyugin L. S., 2000, A&A, 362, 325
Pilyugin L. S., 2001, A&A, 369, 594
Rejkuba M., Da Costa G. S., Jerjen H., Zoccali M., Binggeli B., 2006, A&A, 448, 983
Richer M. G., McCall M. L., 1992, AJ, 103, 54
Richer M. G., McCall M. L., 1995, ApJ, 445, 642
Rönnback J., Bergvall N., 1995, A&A, 302, 353
Sakai S., Madore B. F., Freedman W. L., 1997, ApJ, 480, 589
Schaerer D., Vacca W. D., 1998, ApJ, 497, 168
Schmidt M., 1963, ApJ, 137, 758
Searle L., Sargent W. L. W., 1972, ApJ, 173, 25
Shaw R. A., Dufour R. J., 1995, PASP, 107, 896
Skillman E. D., 1985, ApJ, 290, 449
Skillman E. D., 1989, ApJ, 347, 883
Skillman E. D., 1998, in Aparicio A., Herrero A., Sánchez F., eds, Stellar Astrophysics of the Local Group: VIII Canary Islands Winter School of Astrophysics. Cambridge Univ. Press, Cambridge, p. 457
Skillman E. D., Kennicutt R. C., Jr, Hodge P., 1989, ApJ, 347, 875
Skillman E. D., Côté S., Miller B. W., 2003a, AJ, 125, 593
Skillman E. D., Côté S., Miller B. W., 2003b, AJ, 125, 610
Stasińska G., Comte G., Vigroux L., 1986, A&A, 154, 352
Storey P. J., Hummer P. J., 1995, MNRAS, 272, 41
Strobel N. V., Hodge P., Kennicutt R. C., Jr, 1991, ApJ, 383, 148
Tully R. B., 2005, ApJ, 618, 214
Tully R. B., Somerville R. S., Trentham N., Verheijen M. A. W., 2002, ApJ, 569, 573
van den Bergh S., 1999, ApJ, 517, L97
van Gorkom J. H., van der Hulst J., Haschick A., Tubbs A., 1990, AJ, 99, 1781
van Zee L., 2001, AJ, 121, 2003
van Zee L., Haynes M. P., 2006, ApJ, 636, 214
van Zee L., Haynes M. P., Salzer J. J., 1997, AJ, 114, 2479
van Zee L., Salzer J. J., Haynes M. P., O'Donoghue A. A., Balonek T. J., 1998, AJ, 116, 2805
van Zee L., Skillman E. D., Haynes M. P., 2004a, AJ, 128, 121
van Zee L., Barton E. J., Skillman E. D., 2004b, AJ, 128, 2797
van Zee L., Skillman E. D., Haynes M. P., 2006, ApJ, 637, 269
Webster B. L., Smith M. G., 1983, MNRAS, 204, 743
Webster B. L., Longmore A. J., Hawarden T. G., Mebold U., 1983, MNRAS, 205, 643

This paper has been typeset from a TEX/LATEX file prepared by the author.